Journal of Materials Chemistry C

Revisiting the non-fluorescence of nitroaromatics: presumption versus reality

Journal:	*Journal of Materials Chemistry C*
Manuscript ID	TC-REV-11-2021-005423.R2
Article Type:	Review Article
Date Submitted by the Author:	18-Jan-2022
Complete List of Authors:	Sadowski, Bartłomiej; Polish Academy of Sciences Institute of Organic Chemistry, X Poronik, Yevgen; Polish Academy of Sciences, Institute of Organic Chemistry Szychta, Kamil; Polish Academy of Sciences Institute of Organic Chemistry, X Quina, Frank; University of Sao Paulo, Department of Chemistry Vullev, Valentine; University of California, Riverside, Department of Bioengineering Gryko, Daniel; Instytut Chemii Organicznej PAN

ARTICLE Journal Name

Revisiting the non-fluorescence of nitroaromatics: presumption versus reality

Received 00th January 20xx,
Accepted 00th January 20xx

DOI: 10.1039/x0xx00000x

Yevgen M. Poronik,[a] Bartłomiej Sadowski,[a] Kamil Szychta,[a] Frank H. Quina,[b]* Valentine I. Vullev,[c,d,e]* and Daniel T. Gryko[a]*

The electronically excited singlet states of nitroaromatic compounds are often presumed to be essentially non-fluorescent. Nonetheless, a growing number of reports in the literature have demonstrated that certain structural types of nitroaromatics can indeed fluoresce, and often quite efficiently. Consideration of the mechanisms responsible for the typical fast or ultrafast non-radiative deactivation of the excited singlet states of nitroaromatics points to several general principles for their design that combine the strong electron-withdrawing properties of the nitro group with reasonable fluorescence quantum yields. An overview of published examples of fluorescent nitroaromatics emphasizes these concepts in the context of the importance of chromophore architecture and conformation and the defining roles of excited state charge transfer and solvent polarity in modulating the non-radiative decay channels that compete with fluorescence. Overcoming the stigma that nitroaromatics are intrinsically destined to be non-fluorescent thus paves the way for incorporating the strongly electron-withdrawing nitro group into the existing toolbox for the development of new nitro-substituted fluorophores and chromophores tuned to specific applications.

Introduction

The advent of carbon-based electronics and energy materials places a demand for electron-deficient organic conjugates that can serve as *n*-conducting media, electron acceptors and photooxidants.[1-4] As inherent reductants, a huge diversity of organic structures are available as building blocks for *p*-type materials. In comparison, examples of *n*-type organic conjugates are relatively few and far between.[5] In principle, the nitro group (-NO_2) would be an immensely attractive substituent for electron-deficient conjugates and *n*-conducting materials, as indicated, for example, by the large positive values of its Hammett constants (i.e., σ_p = 0.78 and σ_m = 0.71) and Swain-Lupton parameters (i.e., $\mathscr{F}$ = 0.65 and $\mathscr{R}$ = 0.13).[6] Other widely used electron-withdrawing groups do not quite measure up to -NO_2 in this regard. Thus, for -CN, σ_p = 0.66, σ_m = 0.56, $\mathscr{F}$ = 0.51 and $\mathscr{R}$ = 0.15; for -CF_3 σ_p = 0.54, σ_m = 0.43, $\mathscr{F}$ = 0.38 and $\mathscr{R}$ = 0.16; and for -CO_2CH_3 σ_p = 0.45, σ_m = 0.37, $\mathscr{F}$ = 0.34 and $\mathscr{R}$ = 0.11. Nitro groups induce positive shifts in the reduction potentials of polycyclic aromatic hydrocarbons, such as pyrene and naphthalene, that can exceed 1 V.[7,8] In comparison, the shifts induced by nitrile and carbonyl substituents range between 0.2 and 0.7 V.[9] The attachment one or more nitro groups to the rings of an aromatic compound induces bathochromic spectral shifts, which is potentially an attractive means of shifting the optical absorption from the UV to the visible region of the spectrum or even from the blue to the red or near-infrared regions. Although there are substituents such as -N_2^+ (σ_p = 1.91, σ_m = 1.76, $\mathscr{F}$ = 1.58 and $\mathscr{R}$ = 0.33), -IF_4 (σ_p = 1.15, σ_m = 1.07, $\mathscr{F}$ = 0.98 and $\mathscr{R}$ = 0.17), and -SF_3 (σ_p = 0.80, σ_m = 0.70, $\mathscr{F}$ = 0.63 and $\mathscr{R}$ = 0.17) that are more strongly electron-withdrawing than -NO_2, the resulting compounds are either chemically unstable and/or synthetically challenging.

The downside of nitroaromatics, particularly for photonic and optoelectronic applications, is that their electronically excited singlet states usually exhibit very short lifetimes in the sub-ns and often sub-ps time range.[10-12] Such short lifetimes render the use of nitroaromatics impractical for efficient light-emitting applications and have reinforced the long-standing presumption that they are effectively non-fluorescent. Despite this stigma with regard to their fluorescence, reports in the literature demonstrate that many nitroaromatics can indeed fluoresce, albeit with fluorescence quantum yields (ϕ_f) that are often smaller than about 10^{-3} to 10^{-4}.[10, 12] As a counterexample, however, amine derivatives of nitrobenzoxadiazole (NBD) are sufficiently fluorescent that they have been widely used as fluorescence probes in molecular biology and biochemistry.[13]

Intersystem crossing (ISC) leading to triplet formation, $S_1 \rightarrow T_{1+j}$, is the most prevalent and efficient way by which nitro groups quench fluorescence.[10, 12] Introducing charge-transfer (CT) character in the excited states decreases spin orbit coupling (SOC) and can prove beneficial for increasing lifetimes of the S_1 states of nitroaromatics and making them fluorescent.[10] It is no wonder, therefore, that the few well known fluorescent nitroaromatics contain electron-donating groups or electron-rich condensed aromatic rings that act as electron donors.

Polar media, however, quench the emission of fluorescent nitroaromatics with push-pull or acceptor-donor-acceptor configurations.[10] While introducing CT character to the excited states can suppress ISC, solvent polarity stabilizes such polarized states, bringing them closer to the ground state and opens pathways for efficient internal conversion (IC) *via* back CT. To make nitroaromatics fluoresce, therefore, it is crucial to

[a] Institute of Organic Chemistry, Polish Academy of Sciences, Kasprzaka 44/52, 01-224 Warsaw, Poland. Email: dtgryko@icho.edu.pl
[b] *Instituto de Química, Universidade de São Paulo, Av. Lineu Prestes 748, Cidade Universitária, São Paulo 05508-000, Brazil*. E-mail: quina@usp.br
[c] Department of Bioengineering, University of California, Riverside, 900 University Ave., Riverside, CA 92521, USA. Email: vullev@ucr.edu
[d] Department of Chemistry, University of California, Riverside, 900 University Ave., Riverside, CA 92521, USA.
[e] Department of Biochemistry, University of California, Riverside, 900 University Ave., Riverside, CA 92521, USA.

See DOI: 10.1039/x0xx00000x

introduce just enough CT character in their excited states in order to suppress triplet formation, but not to open alternative routes for non-radiative deactivation.

Tuning the CT character of the excited states by decreasing the electron-donating strength of the chromophore core allows for nitroaromatics which fluoresce, even when in polar media.[11] Such optimization, which suppresses ISC and the formation of strongly polarized CT states, however, can lead to the emergence of alternative pathways of non-radiative deactivation involving the adiabatic transition to singlet nπ* dark states and *aborted photochemistry*.[11]

These multiple layers of complexity that are responsible for the effects of nitro groups on the excited-state dynamics of organic compounds are the underlying reason why *a priori* prediction of the emissive properties of nitroaromatics is neither trivial nor straightforward. Key to the development of structural paradigms for the rational design of fluorescent nitro-substituted dyes with greatly increased ϕ_f and much longer singlet-excited-state lifetimes, τ_s, is an understanding of the photophysics and photochemistry that conspire to make nitroaromatics non-fluorescent.

With this objective in mind, the current review begins with an overview of the mechanisms responsible for the typical femtosecond to picosecond non-radiative deactivation of the emissive excited states of nitroaromatics. This mechanistic understanding allows us to postulate several general principles for the design of nitroaromatics that should be pronouncedly fluorescent but still embody the strong electron-withdrawing properties of the nitro group. Finally, these postulated design principles are validated *via* a survey of published examples of fluorescent nitroaromatics. Overcoming the stigma that nitroaromatics are intrinsically non-fluorescent, this review paves the way for the development of new nitrosubstituted chromophores tuned for applications as synthetic electron deficient dyes, pigments and materials

Non-radiative deactivation induced by nitro groups

Intersystem crossing

Photoexcited nitroaromatic compounds are notorious for forming triplets with high quantum yields. Therefore, a brief overview of ISC will set the foundation for discussing why most nitroaromatics are not strongly fluorescent. In aromatic molecules, the requirements for a fast rate of ISC include: (1) a large spin-orbit coupling (SOC) between singlet and triplet states; (2) a small energy difference between the singlet and triplet states (the energy gap law); and (3) a large number of triplet states lying energetically below the S_1 state.

SOC is a relativistic phenomenon arising from the interaction between the magnetic momenta due to the spin of the electron itself and to the orbital motion of the electrons around the nucleus. For transitions between weakly coupled singlet and triplet manifolds, Fermi's Second Golden Rule provides an expression for the ISC rate constant, k_{ISC} (eq. 1):

$$k_{ISC} = \frac{2\pi}{\hbar}\sum_f \left|\langle\psi_f|\hat{\mathcal{H}}_{SO}|\psi_i\rangle\right|^2 \delta(E_i - E_f) = \frac{2\pi}{\hbar}\sum_f \left|\langle\psi_f|\hat{\boldsymbol{\mathcal{H}}}_{SO}|\psi_i\rangle\right|^2 \delta(\Delta E) \quad (1)$$

where Ψ_i and $\mathcal{E}_i$ are the wavefunction and energy, respectively, of the initial state, typically S_1, and Ψ_f and $\mathcal{E}_f$ are the wavefunctions and energies of the energetically accessible ($\mathcal{E}_f \leq \mathcal{E}_i$) final states, T_j. The delta function represents a requirement for energy conservation and $\hat{\mathcal{H}}_{SO}$ is the (purely electronic) SOC operator. The lack of dependence of SOC on the vibrational modes allows expressing the rate constant in terms of the square of the electronic coupling and a Franck-Condon (FC) factor (Eq. 2):

$$k_{ISC} = \frac{2\pi}{\hbar}\sum_f \left|\langle\psi_f|\hat{\boldsymbol{\mathcal{H}}}_{SO}|\psi_i\rangle\right|^2 \sum_{u,v} \left|\langle\chi_{fu}|\chi_{iv}\rangle\right|^2 \delta(\mathcal{E}_{iv} - \mathcal{E}_{fu}) = \frac{2\pi}{\hbar}\sum_f \left|\langle\psi_f|\hat{\boldsymbol{\mathcal{H}}}_{SO}|\psi_i\rangle\right|^2 F \quad (2)$$

where ψ and χ are the electronic and nuclear wavefunctions, respectively. In this case (Eq. 1), the spin-orbit operator, $\hat{\boldsymbol{\mathcal{H}}}_{SO}$, corresponds only to the direct SOC interaction between the states involved in the ISC, which depends solely on their electronic characteristics.

The direct SOC interactions can involve both single-electron and multielectron interactions. The former represents the interaction between the spin magnetic moment of an electron with that arising from its own orbital motion. This single-electron SOC contribution vanishes for ISC between π,π* states of planar aromatic hydrocarbons, but becomes increasingly important with increasing nuclear charge, emerging as a *heavy-atom effect* that catalyzes the efficient ISC of, for example, bromo- or iodo-substituted aromatic hydrocarbons. The multielectron SOC contributions, on the other hand, arise from interactions between electron spin and the magnetic momenta of the other orbitals. These interactions are responsible for ISC in planar aromatic hydrocarbons without heavy atom substituents. In addition to these direct SOC pathways, $\hat{\boldsymbol{\mathcal{H}}}_{SO}$ can also include spin-vibronic coupling interactions in the singlet and or the triplet manifolds, and vibrationally-enhanced SOC between the singlet and triplet excited state potential surfaces.[14]

The nature of the initial and final electronic states is immensely important for determining the strength of the SOC, as summarized by *El Sayed's rules*.[15-17] Specifically, ISC between excited states with different orbital origins, such as $^1\pi\pi^* \rightarrow {}^3n\pi^*$ and $^1n\pi^* \rightarrow {}^3\pi\pi^*$, is considerably more probable than ISC between states with the same or similar electronic configuration, e.g., $^1\pi\pi^* \rightarrow {}^3\pi\pi^*$ and $^1n\pi^* \rightarrow {}^3n\pi^*$. For organic molecules composed of light atoms, the n orbitals usually have a mixed s and p character. During ISC in the excited state, the electron in the π* orbital remains where it is, while the electron in an n or π orbital has to move to the singly occupied π or n orbital, respectively, in order to compensate for the change in momentum due to the spin flip.

In the high-temperature limit, where the energies of the vibrational modes responsible for the ISC transition do not exceed k_BT, the nuclear contributions to k_{ISC} can be represented by a continuous Gaussian expression for the weighted FC density of states (identical to that in Marcus transition-state theory) (eq. 3):[14, 18]

$$FC = \frac{1}{\sqrt{4\pi\lambda k_BT}}\exp\left(-\frac{(\lambda-\Delta E)^2}{4\lambda k_BT}\right) \quad (3)$$

Despite the striking similarity of eq. 3 to the formalism of Marcus transition-state theory, ISC between nested states does not proceed through a transition state. Instead, ISC couples the initial state, S_1, with quasi-isoenergetic upper vibrational levels of the final state(s), T_j, in the triplet manifold. In the weak SOC limit, with little or no change in nuclear geometry during ISC, the reorganization energy (λ) is small, with the initial state nested into the final states. In this case, the potential-energy surfaces (PESs) of the initial singlet state and the final triplet state(s) have minima at similar nuclear coordinates and do not intersect (Fig. 1)[17]. A reorganization energy, λ, smaller than the energy separation, $\Delta\mathcal{E} = \mathcal{E}_i - \mathcal{E}_f$, between the states results in an inverted-region-type behavior, which is consistent with the *energy-gap law*, i.e., the rate of ISC decreases approximately exponentially as the energy difference $\Delta\mathcal{E}$ increases.

With Plotnikov's approximation for calculating k_{ISC}, the nuclear contributions to the rate can assume the following form (eq. 4): [8, 19, 20]

$$FC = \sum_n \prod_v \frac{e^{-S} S^{n_v}}{n_v!} \quad (4)$$

where the Huang-Rhys factor, S, accounts for the shift of the equilibrium position of the normal modes, and n_v is an integer approximation of the ratio between the singlet-triplet energy difference and the energy of the receiving vibrational mode, i.e., $n_v \approx \Delta\mathcal{E}\ (\hbar\ \omega_v)^{-1}$. With S usually smaller than 1, [8, 20] eq. 2b also predicts a behavior consistent with the *energy-gap law*. On the other hand, a large displacement between the minima of the potential surfaces of the excited singlet and triplet states leads to a substantial reorganization energy and can result in the emergence of crossing points or conical intersections (Fig. 1). In this strong SOC limit, when $\lambda > \Delta\mathcal{E}$, the ISC kinetics follow a normal-region behavior, i.e., an increase in $\Delta\mathcal{E}$ increases k_{ISC}.

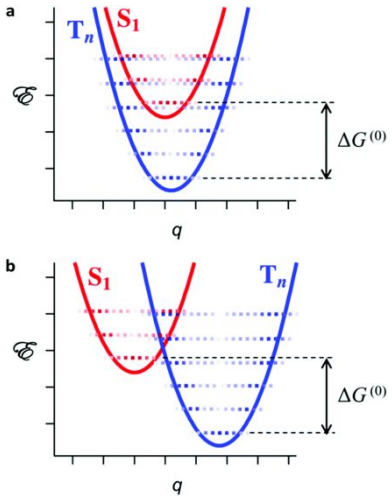

Fig. 1 State diagrams depicting ISC under: (a) weak vibronic coupling, where the nested geometry leads to an overlap between the lowest energy vibrational wavefunction of the S_1 electronic state with the central region of the upper vibrational wavefunctions of the triplet state. (b) Strong vibronic coupling, where vibrational wave functions from the S_1 and T_n electronic sates overlap at the crossings of the potential energy surfaces of the electronic states. Reproduced from ref. [18]

Turning to a consideration of nitroaromatics, the lowest excited singlet state tends to be predominantly π,π* in character, but with nearby n,π* states as well. Although an S_1 and T_1 states of π,π* character should result in rather small SOC, solvation and/or relaxation of the nuclear geometry can alter this order of energy levels and adiabatically change the electronic configuration of S_1 from π,π* to n,π*, promoting strong n,π*/π,π* SOC and thus fast ISC.[11] Moreover, when the molecule has upper triplet states intermediate in energy between S_1 and T_1, the energy gap law points to a preference for intersystem crossing to occur *via* the initial population of these upper triplet states, followed by internal conversion to T_1. Indeed, many nitroaromatics undergo picosecond and sub-picosecond $S_1 \rightarrow T_{1+j}$ ISC, which is faster than the IC within the triplet manifold. As a result, femtosecond pump-probe spectroscopy can resolve the overall transition from S_1 to T_1 states into the two steps of $S_1 \rightarrow T_{1+j} \rightarrow T_1$. Very efficient ISC from the singlet manifold to upper triplet states, $S_1 \rightarrow T_{1+j}$, of the opposite orbital origin are responsible for making most nitroaromatics only weakly fluorescent or even non-fluorescent. Indeed, fluorescence, with rate constants that are usually in the range of ca. 10^7-10^8 s^{-1}, cannot compete with values of k_{ISC} that exceed about 10^{11} s^{-1}, which result in near unit quantum yields of non-radiative decay. In the ground state of many nitroaromatics, such as nitropyrenes and nitronaphthalenes, the nitro groups are almost coplanar with the aromatic rings to which they are attached. As the initially populated π,π* S_1 states of some of them relax, the nitro group can twist out of the plane of the ring and may assume an asymmetric pyramidal geometry, as in 1-nitronaphthalene.[21] This distortion of the nitro group in π,π* S_1 states promotes highly effective transitions to n,π* triplet states with the same geometry.[22] Preventing such distortions of the nitro group can suppress ISC and decreases k_{ISC} by

orders of magnitude.[8] There is still no consensus as to whether it is the pyramidalization, the torsional motion, or the bending and stretching modes of the nitro groups that are responsible for the highly efficient ISC.[10] Nevertheless, constraining the nitroaromatic to be as planar as possible can suppress triplet formation and increase the fluorescence quantum yields.

This paradigm extends to structures of increasing complexity. Introducing the nitro groups as a part of nitrophenyl substituent adds torsional degrees of freedom since the resultant biaryl links can strongly affect the excited-state dynamics.[20] Dyes with *para*-nitrophenyl substituents assume almost planar conformations and can have quantitative fluorescence quantum yields, ϕ_f, in non-polar media.[20] On the other hand, *ortho*-nitro groups in the nitrophenyl substituent prevent coplanarity due to steric hindrance and can increase the ISC rates by orders of magnitude.[20] Orthogonality between aromatic rings increases the overlap between π and σ orbitals that can enhance SOC.[23] In the case of nitrophenyl substituents, the through-space contacts between the n-orbitals on the *ortho* nitro groups and the hole π NTO on the chromophore core provide pathways for strong SOC between S_1 (ππ*) and nπ* T_j states.

Intramolecular charge transfer

The immense electron-withdrawing strength of the nitro groups warrants induction of a CT character in the excited states, which can significantly affect SOC and the ISC rates. Medium polarity augments the alignment between the energy levels of singlet and triplet states if either of them has a CT character, which affects k_{ISC}.

Photoexcitation of 1-nitronaphtalene in a polar solvent, for example, produces a FC S_1 state with a larger dipole than S_0. Thus, in acetonitrile the dipoles of S_0 and the FC S_1 states are 6.6 D and 10 D, respectively.[8] Upon relaxation, the S_1 state loses its CT character while the nitro group twists out of plane and assumes asymmetric pyramidal structure, resulting in $k_{ISC} > 10^{12}$ s^{-1}.[8]

Intramolecular CT can also affect the electronic coupling responsible for direct ISC (eq. 1). CT character in either the triplet or the singlet manifold tends to diminish the SOC between them and hence the rate constant for ISC.[22] In direct ^{1}nπ* ↔ ^{3}ππ* ISC, the particle electron that was promoted to the π* orbital remains in that orbital, while the electron associated with the hole moves from an n and a π orbital (or vice versa) on oxygen. The n orbitals are localized on the oxygens of the nitro group, but the strength of the electronic coupling is a function of the extent of participation of the π orbitals on oxygen of the nitro group in the molecular orbitals involved in the transition. The tendency of intramolecular CT is to localize the natural transition orbital (NTO) of the particle electron on the nitro group and pull the hole NTO over to the π-conjugated aromatic rings, away from the nitro group, resulting in a ππ* CT state. Therefore, enhancing the CT character of the excited state reduces the overlap between the hole and particle NTOs of the states of different multiplicity and weakens the SOC interaction between them.

The existence of strongly fluorescent "push-pull" nitroaromatics containing electron-donating groups or electron-rich polycyclic aromatic moieties[8, 24, 25] is due precisely to the enhancement of the effects of intramolecular CT on the FC singlet state and on the electronic-coupling factors involved in ISC. Several of the fluorescence probes widely used in molecular biology and biochemistry are amine derivatives of nitrobenzoxadiazole (NBD).[26] Replacing the oxygen of the heterocyclic ring of NBD with nitrogen, sulfur, selenium or a quaternary carbon produces a series of strongly fluorescent analogues with emission maxima ranging from the blue to the red.[27]

Introducing a nitro group into a chromophore that is already a good electron donor can also result in a fluorescent push-pull nitroaromatic chromophore. Perylene is a better electron donor than pyrene, by about 0.3 V,[28] and the lowest singlet-excited state of nitroperylene has a pronounced CT character, as evident from the features of the perylene radical cation in its transient-absorption spectra.[29] Compared to 1-nitropyrene, which is virtually non-fluorescent with a picosecond excited-state lifetime, 3-nitroperylene is strongly fluorescent with a nanosecond lifetime.[7, 29]

While beneficial for suppressing ISC, enhancing the CT character of the singlet-excited states can open up alternative, potentially undesirable pathways for non-radiative deactivation and fluorescence quenching. The increased electric dipole moment of an excited state with CT character makes its energy more susceptible to the influence of the polarity of the medium than that of the ground state. Polar solvents stabilize dipolar S_1 states and bring their PESs closer to the PES of S_0 that can create new IC pathways for back CT, often through conical intersections or near crossings between the PESs.[10, 20] This phenomenon can explain the frequently observed medium-polarity-induced quenching of the fluorescence of nitroaromatics in which the shortening of the excited-state lifetime is not accompanied by concomitant population of the triplet state.[10, 20]

Increasing the CT character of the S_1 state can increase the separation between the hole and particle NTOs and hence decrease the overlap between them. This in turn decreases the oscillator strength of the $S_1 \rightarrow S_0$ radiative transition and therefore k_f. For example, adding an electron donating group to the other ring of nitronaphthalene was found to decrease k_{ISC} and increase the lifetime of the fluorescent excited state by several orders of magnitude.[8] Nonetheless, the fluorescence quantum yield remained small, i.e., $\phi_f \lesssim 0.01$.[8]

Conformational changes further modulate these effects of CT on the fluorescence properties of nitroaromatics. In non-polar media, the nitro group of 5-amino-1-nitronaphthlane is not completely twisted out of the plane of the aromatic rings, and k_f is about 6×10^7 s^{-1}, while in polar solvents the nitro group is orthogonal to the rings and k_f decreases by ca. two orders of magnitude.[8] In contrast, replacing the amine by a weaker electron-donating N-amide group increases k_f to 10^8 s^{-1} and eliminates the solvent-polarity dependence of k_f and, except for a small decrease in a moderately polar solvent like dichloromethane, the rate of competitive nonradiative decay.[8]

This example illustrates the multifaceted complexity of CT effects and the importance of appropriately tuning the degree of CT character introduced into the excited states.

A key design strategy for producing fluorescent nitroaromatics is to attach the nitro group to the chromophore of interest as a nitrophenyl and related nitroaryl substituent rather than forming a direct bond between NO_2 and the chromophore.[20] The effects of dihedral rotation of the attached nitroaryl substituent on k_{ISC}, k_f and non-radiative decay (k_{nd}) are quite similar to those of rotation of nitro groups attached directly to the chromophore. Molecules with small or moderate dihedral angles between the nitrophenyl group and the chromophore can be fluorescent and exhibit pronounced solvatochromism. However, a much larger dihedral angle that isolates the particle NTOs on the nitrophenyl moiety from the hole NTOs on the chromophore results in a twisted intramolecular charge transfer (TICT) species. TICT states are typically dark excited states that undergo efficient IC to S_0, especially in polar solvents[30] Formation of TICT states can also enhance ISC to the point that it dominates over other non-radiative-deactivation pathways. Moving the nitro group from *para* or *meta* to the *ortho* position not only forces orthogonality of the nitrophenyl substituent, but also can increase k_{ISC} by several orders of magnitude.[20]

Increasing the number of nitro groups attached to a chromophore can occasionally prove to be beneficial for enhancing fluorescence. In a report of the synthesis of a highly symmetrical 3.7-diamino-1,5-dinitronaphthalene, for example, "recrystallization from acetonitrile gave dark prisms with greenish fluorescence."[31] Assembling nitrophenyl acceptors and an electron-rich aromatic donor to produce acceptor-donor-acceptor (ADA) configurations has been shown to result in fluorescent conjugates.[11, 32, 33] The quadrupole symmetry of the ground and FC excited states of such ADA dinitroaromatics precludes solvatochromism in the absorption spectrum, i.e., $S_0 \rightarrow S_1^{(FC)}$. However, asymmetric CT between the electron-rich core and one of the nitrophenyls in the excited state breaks the quadrupole symmetry and results in a huge increase in the electric dipole moment[34, 35]. Dimers of nitroaromatics can also assume quadrupole symmetry in their ground states that breaks upon photoexcitation.[8] An increase in the solvent polarity approximates the PESs of the CT state and S_0, causing solvatofluorochromism (a bathochromic shifts of the fluorescence, but not of the absorption spectrum). At the same time, polar solvents enhance the non-radiative deactivation rates (IC and sometimes ISC) and reduce the $S_1 \rightarrow S_0$ oscillator strength and k_f. Highly polar solvents induce adiabatic transitions to a non-fluorescent TICT state for such ADA *bis*-nitrophenyl aromatics.[20]

Unique features of the nitro group

The effects of substituents on the excited state properties of simple benzene derivatives point to several important distinctions between the nitro group and other substituents. As a general trend, readily oxidizable and strongly electron-donating substituents such as amines, with very negative Hammett σ_p values, preferentially raise the energy of the highest occupied molecular orbital (HOMO), while readily reducible and electron-withdrawing substituents such as -$COCH_3$ and -NO_2, with large positive Hammett σ_p values, preferentially lower the energy of the lowest unoccupied molecular orbital (LUMO).[36-39]. An interesting comparison is between -NO_2 and -CO_2^- as substituents. Although both have similar structures and the same number of electrons, the nitro group is strongly electron withdrawing, while the carboxylate is not (Hammett $\sigma_p = 0$)[6] and aromatic carboxylates are usually quite fluorescent, in contrast to most nitroarenes.

As a 4n+2 π-electron system, benzene is Hückel aromatic in the ground state. Attachment of a nitro group, with its particularly strong inductive electron-withdrawing (*-I*) effect reduces the ground state aromaticity much more than other substituents with smaller inductive *-I* effects, such as esters, aldehydes, ketones and even nitriles.[40] Conversely, 4n+2 π-electron systems, such as benzene, naphthalene and anthracene, are antiaromatic in the lowest triplet excited state, T_1,[41-43] as well as to a large extent in the lowest singlet excited state.[44] In the case of nitrobenzene, benzaldehyde and acetophenone, however, with the strongly electron-withdrawing substituents -NO_2, -CHO and -$COCH_3$, T_1 recovers aromatic character in the form of an $^3n\pi^*$ state with localization of the electron spin density on the substituent (-NO_2) or partially on the substituent and on the para-carbon of the ring (-CHO and -$COCH_3$).[42] In contrast, the $^3\pi\pi^*$ T_1 states of benzonitrile, benzoic acid, methyl benzoate and benzamide, without similarly low-lying $^3n\pi^*$ states, retain their antiaromatic character.

In polycyclic nitroarenes such as nitronaphthalenes[22] and nitropyrenes,[7] the lowest energy singlet (S_1) and triplet (T_1) excited states are predominantly $\pi\pi^*$ in nature, with a nearby $^1n\pi^*$ S_2 state and an $^3n\pi^*$ upper triplet state (T_j) intermediate in energy between T_1 and S_1. Excited state dynamics, involving, for example, torsional modes of the nitro group that modify its conjugation with the π´system and perhaps its propensity to circumvent antiaromaticity, can result in an inversion of the relative energies of the $^1n\pi^*$ and $^1\pi\pi^*$ states in the singlet manifold. In accord with El Sayed's rules, the two paths that potentially permit fast ISC are from the initial $^1\pi\pi^*$ state *via* the intermediate $^3n\pi^*$ T_j state (followed by IC to T_1) and from the relaxed $^1n\pi^*$ state directly to the $^3\pi\pi^*$ T_1 state. In the particular case of 2-nitronaphthalene, the latter pathway is the more important of the two ISC routes.[22] As in the case of carbonyls, the major contribution to spin-orbit coupling in the nitro group comes from the one-center term between the $n \leftrightarrow \pi$ orbitals localized on the oxygen atoms. Among other common electron-withdrawing substituents, only arene chromophores conjugated with aldehyde and keto groups have similarly low-lying $^1n\pi^*$ states. Consequently, arenes substituted with other commonly employed electron-withdrawing substituents without such low-lying $n\pi^*$ singlet or triplet states, such as cyano, trifluoromethyl, and sulfonate or carboxyl and their derivatives, are typically much more fluorescent due to the much larger fluorescence rate

constants, k_f, of $^1\pi\pi^*$ singlet states combined with much slower ISC between $^1\pi\pi^*$ singlet and $^3\pi\pi^*$ triplet states.

The property that clearly sets the nitro group apart from carbonyl groups is the notable difference in their susceptibilities to specific hydrogen-bonding interactions with polar protic solvents in the ground and excited states. Although the nitro group has higher electron density (especially in excited states with CT character) than carbonyl substituents, carbonyl oxygens are much better hydrogen-bond acceptors than $-NO_2$. In fact, in the ground state nitrobenzene is an even poorer hydrogen-bond acceptor than acetonitrile, as indicated in the following sequence of Abraham parameters for solute hydrogen bond basicity (B), which provide a more quantitative appreciation of the modest (at best) hydrogen-bonding propensity of the nitro group: benzene (0.10), naphthalene (0.20), anthracene (0.26), nitrobenzene (0.28), acetonitrile (0.32), benzonitrile (0.33), benzaldehyde (0.39), benzoic acid (0.40), methyl benzoate (0.46), acetophenone (0.48) and benzamide (0.67).[45] Thus, for example, a change in solvent from acetonitrile to methanol does not significantly increase k_{ISC} of nitropyrene or its derivatives.[7, 46] Alkanoylpyrenes, on the other hand, are non-fluorescent in aprotic solvents but become strongly fluorescent in protic media[47, 48] due to hydrogen bonding of the protic solvent to the n-electrons of the carbonyl oxygen.[47] This bonding increases the energies of both the singlet and triplet $n\pi^*$ states, transforming S_1 of the alkanoylpyrene into an intrinsically more fluorescent $^1\pi\pi^*$ state. At the same time, the energy of the $^3n\pi^*$ state increases above that of S_1, making the much faster $^1\pi\pi^* \rightarrow {}^3n\pi^*$ ISC pathway energetically inaccessible.

In summary, because closely situated potential energy surfaces of $^1\pi\pi^*$ and $^1n\pi^*$ states provide pathways for efficient triplet formation, the key to making nitroaromatics fluorescent is to find ways of partially or completely circumventing these pathways without introducing other competitive decay modes, such as conical intersections between PESs. Alternatives that can serve to uncouple, at least partially, the substituent from the aromatic ring to which it is attached, such as: (1) introducing the nitro groups as nitroaryl substituents; (2) placing the nitro group at a position on the aromatic ring characterized by a nodal plane in both S_0 and S_1, and (3) using steric hindrance with neighboring substituents to force the nitro group into near orthogonality with respect to the plane of the ring. Although nitro groups are poor hydrogen bond acceptors, their strong electron-withdrawing character typically results in both a ground state molecular dipole moment and a reasonable change in the dipole moment upon excitation of nitroarenes due to intramolecular CT. Consequently, the CT character and energies of the excited states of nitroarenes are susceptible to the influence of dipole-dipole interactions with the solvent. At the same time, by judiciously incorporating electron-donating moieties to produce tailored push-pull nitroarenes, the CT character of the excited states can be tuned, in consonance with solvent polarity, to produce highly fluorescent nitroarenes, as amply documented in the review of the experimental literature below.

Suppressing intersystem crossing in moderately polar solvents

The in-depth analysis of the literature has revealed that among the fluorescent nitro-aromatics there are two major scenarios of the dependence of fluorescence intensity on solvent polarity, which originates from the interplay between ISC and CT once the molecules reach their S_1 states. (1) Majority of the fluorescent nitroaromatics show noticeably large emission quantum yields when in non-polar solvents; and an increase in the medium polarity quenches their fluorescence. (2) A few examples of dyes, however, show fluorescence intensity that is low in non-polar solvents, reaches a maximum in media of intermediate polarity and then (usually) decreases in highly polar solvents. We will start by presenting what is known about these latter cases.

Aromatic compounds bearing the nitro group in any event exhibit a polarized molecular structure as the nitro group is strongly electron-withdrawing. Consequently, among fluorescent nitroaromatics, the polarized chromophores make up a significant part, where typically, the nitro group is accompanied by an auxiliary electron-donating moiety. The simplest donor-acceptor nitroaromatics, such as 4-nitroaniline, 4-amino-4'-nitrobiphenyl and related compounds, are useful models for which the photophysical processes have been studied.[49-58]

As the mutual conformation of the two benzene rings in the biphenyl moiety obstructs the possibility of strong conjugation between the donor and the acceptor moieties, introduction of a vinyl linker can be used to maximize planarity.

Nitrostilbenes possessing the dipolar structure have been studied since the 1950's, along with stilbenes containing other electron-withdrawing groups. Nitro-stilbenes were reported to exhibit fluorescence properties,[59] though polarized stilbenes with electron-withdrawing groups other than the nitro group showed much stronger fluorescence responses. Nevertheless, quantitative fluorescence studies of nitrostilbenes were reported in the 1970's. Since then, many studies have enhanced the family of dipolar nitrostilbenes and provided insight into how external influences affect the fluorescence response.[60-62]

According to a uniform model on nitrostilbenes[63-67] the fluorescence occurs mainly through radiative relaxation from the $^1LE^*$ state. In non-polar solvents, concurrent to emission the $^1LE^*$ state mainly undergoes ISC, resulting in *trans-cis* isomerization. Solvents of intermediate polarity lower the energy of the $^1LE^*$ state, thus making emission a more favorable relaxation pathway. In highly polar solvents, the CT state with twisted geometry becomes dominant, giving rise to a dramatic fluorescence decrease due the fast decay *via* a radiationless pathway.[68]

This model applies well to all nitrostilbenes with additional amino (**1**-**5**),[63-65] hydroxy (**6**, **7**)[66] and alkoxy (**8**, **9**)[67] electron-

donor moieties (Fig. 2). The absorption properties of nitrostilbenes are characterized by a weak positive solvatochromism with maxima located in the 370-450 nm region depending on solvent polarity. The strength of the electron-donor group does not affect the absorption properties, however, the fluorescence properties, including the spectral ranges and responses, are strongly dependent on both the electron-donor strength and the solvent polarity. Commonly, more polarized chromophores show stronger fluorescence responses, i.e., stilbenes **1**-**5** with amino groups tend to show stronger fluorescence than hydroxystilbenes **6**, **7** or alkoxystilbenes **8**, **9** (Table 1).

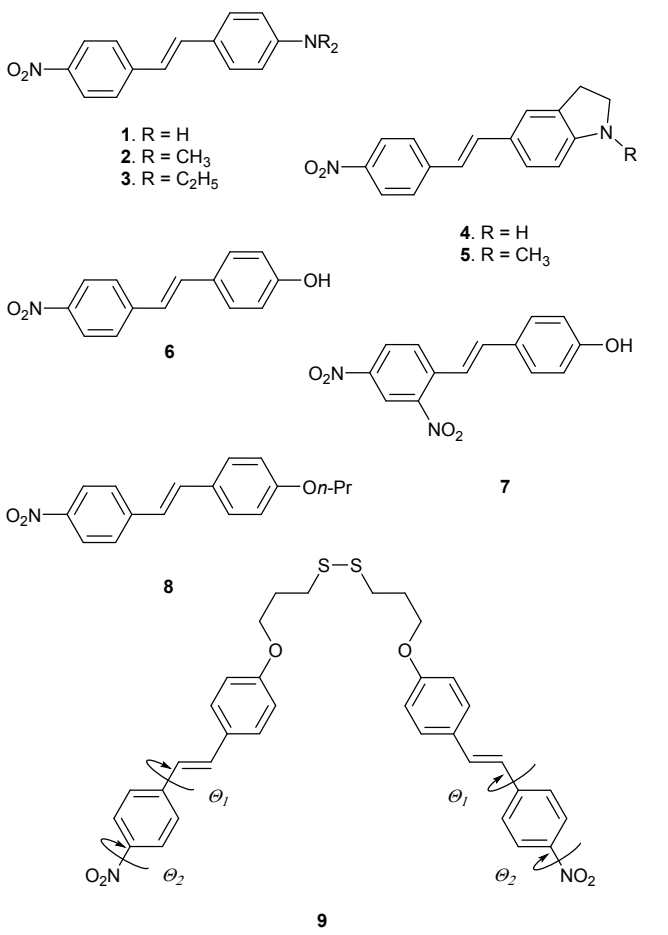

Fig. 2 Structures of nitrostilbenes **1**-**9** possessing different electron donors

Table 1 Fundamental photophysical properties of dyes **1-9** in a range of solvents.

	$E_T^N(30)$ / kcal/mol	**1**		**2**		**3**		**4**		**5**		**6**		**8**		**9**	
		λ_{abs} /nm	λ_{em} /nm (Φ_f) [Φ_{ISC}]	λ_{abs} /nm	λ_{em} /nm (Φ_f) [Φ_{ISC}]	λ_{abs} /nm	λ_{em} /nm (Φ_f)	λ_{abs} /nm	λ_{em} /nm (Φ_f)	λ_{abs} /nm	λ_{em} /nm (Φ_f)	λ_{abs} /nm	λ_{em} /nm (Φ_f)	λ_{abs} /nm	λ_{em} /nm (Φ_f) [Φ_{ISC}]	λ_{abs} /nm	λ_{em} /nm (Φ_f)
n-C_5H_{12}		370	440 (0.004)	411	465 (0.14)	418	470 (0.28)	400	470 (0.12)	410	485 (0.38)						
C_6H_{12}	31.2	380	445 (0.002) [0.8][62]	417	470 (0.33) [0.45][62]	427	478 (0.34)	408	475 (0.20)	420	495 (0.40)			357, 369	408, 420 (<10^{-4}) [0.89][a, 62]		
CCl_4	32.5	390	514 (0.20)	423	548 (0.40)	429	556 (0.50)	412	559 (0.40)	426	578 (0.50)						
m-xylene	33.3	398	544 (0.37)	428	570 (0.55)	434	580 (0.53)	419	590 (0.50)	430	605 (0.55)						
toluene	33.9	399	554 (0.42) [0.2][62]	428	583 (0.53) [0.05][62]	438	589 (0.50)	426	600 (0.45)	433	619 (0.40)	372	490 (<0.0005)			373	491 (0.0008)
C_6H_6	34.5	398	558 (0.48) [0.2][62]	429	596 (0.53) [0.05][62]	439	595 (0.54)	424	607 (0.46)	437	627 (0.40)				[0.9][a, 62]		
Et_2O	34.6	402	590 (0.47)	422	602 (0.55)	430	602 (0.60)	418	635 (0.33)	428	640 (0.45)			368	476 (0.0005)	365	482 (0.0008)
dioxane	36.0	404	598 (0.38)	424	620 (0.32)	434	621 (0.55)	422	630 (0.25)	432	660 (0.35)				[0.9][a, 62]		
THF	37.4	411	647 (0.17)	426	670 (0.11)	442	670 (0.15)		696 (0.04)	435	725 (0.05)			375	515 (0.052)	373	525 (0.0938)
EtOAc	38.1	406	648 (0.15)	424	674 (0.06)	434	680 (0.11)		702 (0.03)	428	720 (0.03)	375	535 (0.091)	373	521 (0.04)	368	523 (0.058)
$CHCl_3$	39.1	399	682 (0.05)	434	735 (0.018)	447	785 (0.023)			438	770 (0.015)						
CH_2Cl_2	41.1	400	694 (0.038) [<0.1][62]	435	770 (0.008) [0.01][62]	447	820 (0.014)	423	770 (<0.01)	439	850 (0.01)	372	572 (0.24)	379	566 (0.16)	377	586 (0.136)
acetone	42.1	410	740 (0.006)	433	800 (0.005)	441	830 (<0.005)			433	>850 (0.005)			375	559 (0.22)	374	577 (0.136)
DMF	43.8	412	830 (0.002) [<0.1][62]	440	850 (0.002)	440	>830 (<0.002)			445	>850 (<0.002)	392	640 (0.031)	383	581 (0.18) [0.11][a, 62]	382	603 (0.139)
CH_3CN	46.0	406		435						432		376	621 (0.11)	375	591 (0.09)	374	615 (0.0488)

[a] - Φ_{ISC} data are collected for an analogue with OCH_3 group instead of O*n*-Pr.

In most cases nitrostilbenes show a weak or moderate fluorescence response in solvents of low polarity. The same is true for nitrostilbenes with alkoxy groups (**8**, **9**), as in this case the excited state cannot be as polarized as with amino groups.

In contrast to compounds **8** and **9**, dye **6** demonstrates a stronger fluorescence response, as there is a possibility of proton dissociation in the excited state induced by solvation of the intermediate and the high polarity.

According to the model,[63-67] in nonpolar solvents $^1LE^*$ states experience fast ISC, resulting in *trans-cis* isomerization, and the fluorescence response is very low (Table 1). In highly nonpolar solvents, the amino derivative **1** shows a tendency for weakened emission in favor of ISC, as manifested by the higher quantum yield of *trans-cis* isomerization.[63] The presence of bulky alkyl substituents on the amino group (**2**, **3**) tends to strengthen the fluorescence in non-polar media. It is apparent that the fluorescence is stronger in the case of more efficient conjugation of the dialkylamino group with the chromophore.

Upon increasing the polarity, the intramolecular charge transfer (ICT) process becomes energetically more favorable, so that the fluorescence occurs from the charge transfer state possessing partially planar character. Typically, the trend of the increase in fluorescence efficiency is analogous for all nitrostilbenes, i.e., it is more significant for stronger electron-donating substituents and less so for weaker electron-donors.[28 31 32]

A further polarity increase leads to a lowering of the energy of the CT state so that a CT state with twisted geometry becomes more stable and decays *via* a fast radiationless pathway. The fluorescence weakening in highly polar media is not due to rotation of the amino group. Analysis of the spectroscopic data suggest that fusing the amino groups in nitrostilbenes **4** and **5** hardly changes the fluorescence behavior in comparison with dyes **1-3,** thus ruling out the possibility that the solvatofluorochromism is a direct function of the amino group rotation (Table 1).

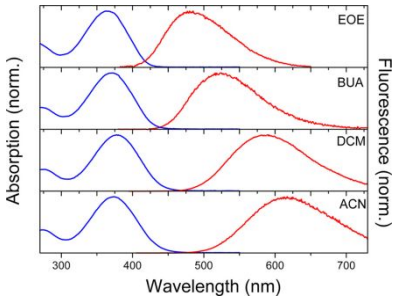

Fig. 3 Absorption (blue) and emission (red) spectra of compound **9** in solvents of different polarity. Reprinted with permission from Ref. [69] Copyright 2012 American Chemical Society.

The spectroscopic behavior of hydroxystilbene **6** is similar to that of its analogues **1**-**5**, **7** and **8**. The fluorescence response in non-polar solvents is weak and the fluorescence efficiency strengthens as the solvent polarity increases. However. in contrast to other nitrostilbenes, it is not as sensitive to the polarity increase. The fluorescence does not dramatically decrease in polar media, going through a maximum as a function of the solvent polarity parameter E_T^N, with the highest value of 0.31 in butyronitrile. A reasonable fluorescence signal is registered in solvents as polar as DMF or acetonitrile. In protic solvents the fluorescence response falls dramatically, most probably due to strong hydrogen bonding interactions.[66] Furthermore, in the presence of bases, hydroxystilbenes experience deprotonation, which induces intramolecular charge transfer in the singlet-excited state. This enhancement of the CT character decreases the energy of the lowest singlet-excited state resulting in an increased rate of internal conversion and hence in fluorescence quenching.[66]

The addition of a second nitro group, as in dinitrostilbene **7**, weakens the fluorescence. Adding a second nitro group enhances the CT character. Furthermore, the nitro group at the *ortho*-position with respect to the vinyl chain causes steric hindrance so that the dinitro aryl moiety or the *ortho*-nitro group alone are partially out of plane, which stabilizes the nonplanar CT state.

Chromophore **9,** a dimer derived from **8,** displays properties similar to the monomeric congener (Fig. 2).[69] After excitation to the planar $^1LE^*$ state, **9** can relax through emission or undergo ISC and the *trans-cis* isomerization that is overwhelming in nonpolar media. The mutual orientation of the nitrophenyl moiety is almost orthogonal. By increasing the solvent polarity, the energy of $^1LE^*$ decreases due to charge transfer stabilization, resulting in growth of its population and higher fluorescence quantum yield (Fig. 3, Table 2).

Table 2 Photophysical data for nitrostilbene **9** at room temperature in various solvents. Reprinted with permission from Ref. 69 Copyright 2012 American Chemical Society.

solvent	λ_{abs} / nm	λ_{em} / nm	$\Delta\bar{\nu}_s$ / cm^{-1}	Φ_f	τ_f / ns	$k_r \cdot 10^{-8}$ / s^{-1} [a]	$k_{nr} \cdot 10^{-8}$ / s^{-1} [b]	$\Phi_{t\to c}$
Et_2O	365	482	6650	0.0008	<0.20			0.36
Toluene	373	491	6443	0.0008	<0.20			0.35
BuOAc	372	514	7426	0.0113				0.31
EtOAc	368	523	8053	0.0580	0.51	1.1	18.5	0.30
THF	373	525	7762	0.0938	0.67	1.4	13.5	0.24
DCM	377	586	9460	0.1360	1.53	0.9	5.6	0.05
Acetone	374	577	9407	0.1360				0.05
DMF	382	603	9594	0.1390	1.94	0.7	4.4	0.03
EtCN	374	595	9931	0.1000				0.04

MeCN	374	615	10478	0.0488	0.95	0.5	10.0	0.03

[a] $k_r = \Phi_f / \tau_f$; [b] $k_{nr} = (1 - \Phi_f) / \tau_f$

The evidence that H-bonding is responsible for fluorescence quenching is represented by the following example. In very polar protic media, H-bonding affects the conformation of **9,** making the nitro groups orthogonal and hence non-conjugated, thereby reducing the fluorescence efficiency. The formation of a 2:1 host-guest complex with *β*-cyclodextrin (*β*-CD) diminishes the H-bonding. It results in a blue shift of the fluorescence maximum, along with a strong increase in the fluorescence response, compared with the free chromophore (Fig. 4).

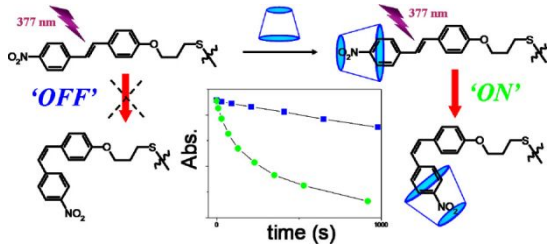

Fig. 4 A host-guest complexe with *β*-cyclodextrin (*β*-CD) diminishes H-bonding, resulting in both a blue-shift of the fluorescence maximum along with an increase in the fluorescence response. Reprinted with permission from Ref. [69] Copyright 2012 American Chemical Society.

Introducing additional linkers can lead to an increase in charge separation. It, however, also enhances the chromophore propensity for twisting.[70]

The structures of the *cis*- and *trans*- derivatives **10** and **11** resemble nitrostilbenes **1**-**9** with two ethyne bridges incorporated into the stilbene chromophore. Compounds **10** and **11** were independently synthesized from the appropriate *Z*- or *E*- isomers of 1,2-dichloroethene using the Heck methodology (Fig. 5).

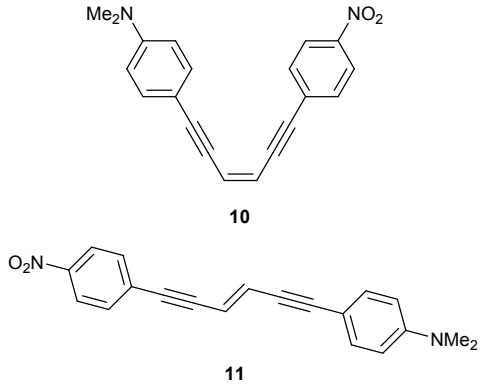

Fig. 5 Structures of the push-pull chromophores **10** and **11**.

These isomers show different absorption spectra matching well the expected spectral shapes for such linear and bent chromophores (Fig. 6).[71]

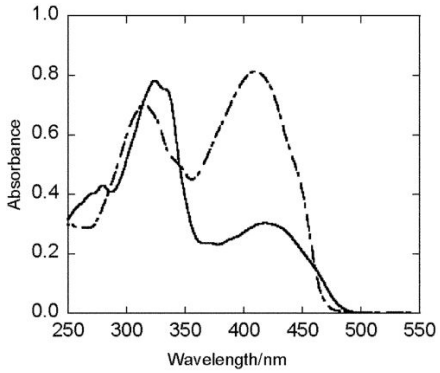

Fig. 6 The absorption spectra of **10** (solid line) and **11** (dot–dash line). Reproduced from Ref.[71]

The fluorescence behavior of the stilbene ethynylogues **10** and **11** is consistent with that of nitro-stilbenes **1**-**9**. Fluorescence was observed only for the *trans*-isomer in nonpolar solvents. Furthermore, **11** showed a moderate fluorescence efficiency in cyclohexane, exhibiting a well resolved fluorescence band with relatively small Stokes shift (Table 3).

Table 3 Photophysical properties of compound **11** in solvent systems of different polarity. Reproduced from Ref.[71]

		λ_{abs}/nm	λ_{em}/nm	$\Delta\bar{\nu}_s$ / cm^{-1}	Φ_f
CH_2Cl_2 (vol %) – C_6H_{12}	0	315, 410	469, 499	3000	0.33
	1	410	479, 500	3500	0.37
	2	411	501	4400	0.40
	4	411	514	4900	0.42
	8	410	541	5900	0.31
	12	411	576	7000	0.13
	16	409	584	7300	0.085
	20	409	601	7800	0.046
	40	411	647	8900	0.004
	60	411	682	9700	0.0004
C_6H_6		325	581	6600	0.25

The fluorescence of **11** is very sensitive to the solvent polarity. Even in benzene it shows a significantly red-shifted fluorescence band with an unresolved vibronic structure and moderate efficiency. On the other hand, further small increases in the solvent polarity (addition of CH_2Cl_2 to cyclohexane) can lead to almost complete loss of fluorescence.

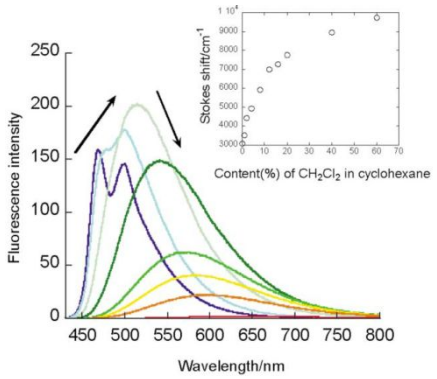

Fig. 7 Fluorescence spectra of **11** in mixed solvents of CH_2Cl_2–C_6H_{12}. CH_2Cl_2 content: 0% (dark blue), 1% (blue), 4% (light blue), 8% (green), 12% (yellowish green), 16% (yellow), 20% (orange), 40% (red) and 60% (dark red). Reproduced from Ref.[71]

Gradual addition of CH_2Cl_2 to a cyclohexane solution of **11** modulates the increase in solvent polarity and allows the determination of the exact point of highest fluorescence efficiency (Table 3, Fig. 7).

Table 4 Spectral and kinetic properties and transient assignments of **12** and **13** in solvents of different polarity based on ultrafast time-resolved absorption spectroscopy at λ_{exc} = 400 nm[a]. Reproduced from Ref. [72]

Solvent	Compound **12**		Compound **13**		Transient
	τ / ps	λ / nm	τ / ps	λ / nm	
Toluene	0.10	580(+), 690(−)	0.18	535(+), 740(+)	Solvation
	1.3	<480(−), 720(+)	1.2	750(+)	Solvation
	12	720(+)	12	740(+)	$^1LE^*$
	180	525(+), 595(+)	160	640(+)	T_1'
	Rest	525(+), 595(+)	Rest	640(+)	T_1
Anisole	1.8	710(+)	0.66	<480(−), 740(+)	Solvation
	8.7	<480(−), 710(+)	6.6	<480(−), 740(+)	$^1LE^*$
	360	700(+)	400	730(+)	$^1ICT^*$
	Rest	525(+), 605(+)	Rest	670(+)	T_1
EtOAc	0.63	<480(−), 700(+)	0.70	<480(−), 730(+)	Solvation
	9.0	505(−), 690(+)	8.1	510(−), 730(+)	$^1LE^*$
	88	520(−), 685(+)	150	735(+)	$^1ICT^*$
	Rest	515(+), 600(+)	Rest	650(+)	T_1
CH_3CN	0.19	<480(−), 700(+)	0.24	<480(−), 705(+)	Solvation
	0.82	670(+)	0.90	730(+)	Solvation
	110	530(+), 650(+)	240	710(+)	$^1LE^*$
	2100	520(+), 650(+)	2100	710(+)	$^1ICT^*$
	Rest	520(+), 625(+)	Rest	635(+)	T_1

[a] Spectral properties refer to species associated spectra (SAS) calculated by target analysis. The symbols (+) and (−) stand for positive and negative signals, respectively.

Similarly to nitrostilbenes the rationale behind the solvatofluorochromism of **11** is fluorescence from a $^1LE^*$ state in nonpolar solvents. Upon increasing the solvent polarity, the ICT mechanism starts to play a significant role, resulting in a red-shift of the fluorescence maximum along with a gradual decrease in the fluorescence efficiency.

Transient absorption spectroscopy (TAS) supports the excited state relaxation model for nitrostilbenes and related compounds. 1,4-Distyrylbenzenes **12**-**14** are formally vinylogues of nitrostilbenes with the chromophore π-expanded by one styryl (vinylbenzene) scaffold, with chromophore **12** featuring a dipolar and dye **13** quadrupolar structures (Fig. 8).[72-75]

The absorption spectra of dyes **12** and **13** exhibit weak positive solvatochromism on going from cyclohexane to polar acetonitrile and DMSO. The analysis of the fluorescence properties on the basis of steady-state and time-resolved fluorescence, ultrafast transient absorption spectroscopy (TAS) and computational techniques shows strict analogy with nitrostilbenes and their analogues.

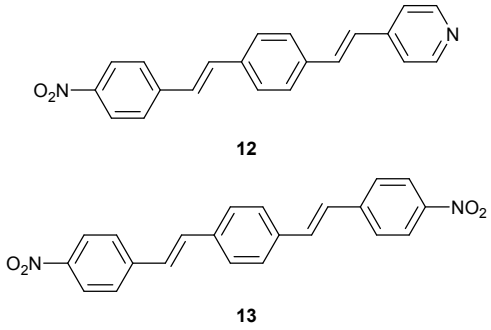

Fig. 8 Structures of nitroaromatics **12** and **13**.

In addition to the computational data which are consistent with nitrostilbenes, in the case of dye **12** both fluorescence spectroscopy and TAS were able to show two types of radiative relaxation. The first corresponded to the $^1LE^*$ and the second to the $^1ICT^*$ stabilized in solvents of higher polarity. Changing the toluene–anisole ratio in the solvent mixture showed the dual nature of the fluorescence (Fig. 9, Table 4).[72] In pure toluene the fluorescence spectrum of **12** shows an emission maximum at 435 nm, while in anisole it shifts to 510 nm. On further polarity increase the fluorescence maxima are red shifted, along with an increase in the fluorescence quantum yield (Table 5). In contrast to nitrostilbenes, even in the most polar solvents the structure of the $^1ICT^*$ state does not lose planarity and the fluorescence is not quenched. According to computational data, an increase in medium polarity lowers the ICT energy, thus, increasing its population in lieu of the triplet state. The fact that compounds **12** and **13** fluoresce from the ICT state is consistent with planarity, or at least partial planarity, of their structures.

Table 5 Photophysical properties of dyes **12**-**13** as a function of solvent polarity at room temperature. Reproduced from Ref. [72]

Solvent	$f(\varepsilon,n)$[a]	**12**						**13**					
		λ_{abs} / nm	λ_{em} / nm	$\Delta\bar{\nu}_s$ / cm^{-1}	Φ_f (Φ_{ISC})	τ_f / ns	$k_f \cdot 10^8$ / s^{-1}	λ_{abs} / nm	λ_{em} / nm	$\Delta\bar{\nu}_s$ / cm^{-1}	Φ_f (Φ_{ISC})	τ_f / ns	$k_f \cdot 10^8$ / s^{-1}
C_6H_{12}	0.0021	375	427	3247	0.00005[b] (0.68)								
Tol	0.0242	382	435	3190	0.0022	0.012[c]	1.8	396	474	3750	0.010 (0.37)	0.012[c]	8.3
Tol/An 7:3	0.0996	382.5	438	3310	0.009			399	475	4010	0.034	0.056	6.1
Tol/An 5:5	0.143	382	462	4530	0.015			399	488	4570	0.074	0.18	4.1

Tol/An 3:7	0.178	384	494	5800	0.030			402	492	4550	0.13	0.33	3.9
An	0.224	385.5	510	6330	0.067	0.32	2.1	403	502	4890	0.22	0.63	3.5
$CHCl_3$	0.293	382	545	7830	0.19	1.7	1.1	400	542	6550	0.46	1.8	2.6
EtOAc	0.400	378	500	6455	0.017	< 0.5	> 0.3	395	496	5155	0.088	0.26	3.4
DCE	0.497	383	555	8092	0.31	1.9	1.6	401	557	6984	0.55	2.0	2.8
CH_3COCH_3	0.651	379	560	8528	0.29	1.8	1.6	398	557	7170	0.51	2.1	2.4
DMSO	0.655	393	608	8998	0.45	1.5	3.0	413	612	7870	0.40	1.9	2.1
DMF	0.667	388	583	8621	0.57	2.5	2.3	407	588	7560	0.56	2.3	2.4
MeCN	0.712	378	594	9620	0.47 (0.30)	2.1[b]	2.2[b]	396	598	8530	0.46 (0.17)	2.1	2.2

[a] $f(\varepsilon,n) = [(\varepsilon - 1)/(\varepsilon + 2)] - [(n^2 - 1)/(n^2 + 2)]$. [b] From ref. 72. [c] From pump-probe measurements

Ultrafast transient absorption experiments support the steady state spectroscopic data. The TAS experiments are in agreement with a transient absorption attributed to $^1LE^*$ and a further short-lived transient corresponding to $^1ICT^*$ (Table 4).[72]The spectra measured in toluene show the formation of bands at 725 and 740 nm for **12** and **13**, respectively, which decay during the first few picoseconds. After that, the spectra show a transient absorbing below 650 nm, corresponding to the triplet state. In contrast, in acetonitrile the $^1LE^*$ state formed after solvation (the transient at around 700 nm) undergoes an ICT, showing a significant blue shift on a longer time scale.

Hence, for stilbene vinylogues **12**-**13** the fluorescence quenching pattern reflects radiationless decay via ISC, which dominates in nonpolar solvents, while the excited state dynamics in polar media facilitate population of a planar $^1ICT^*$, resulting in efficient emission (Tables 4-5).

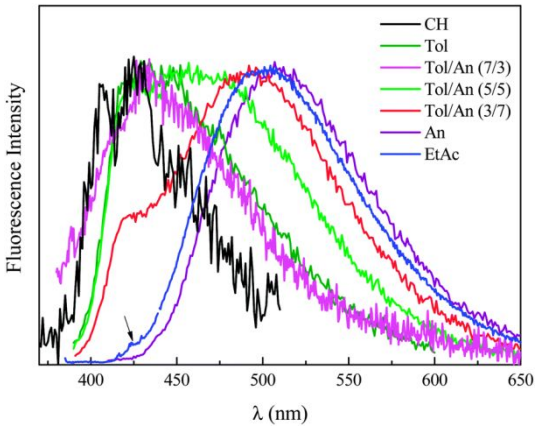

Fig. 9 Normalized emission spectra of **12** in different solvents. Reproduced from Ref. [72]

A modification of nitrostilbene chromophore with heterocycles gives rise to a family of nitroaromatics related to both nitrostilbenes **1**-**9** and compound **13** (Fig. 10). The absorption of dyes **14a,b** and **15a,b** is somewhat blue-shifted compared with **1-5** as aminophenyl moieties tend to show stronger electron donor properties (Tables 1, 6). On the other hand, the absorption maxima are red-shifted in comparison with **13** as furan and thiophene typically provide stronger chromophore polarization. The origin of the fluorescence properties of compounds **14a,b** and **15a,b** comes from the possibility of the formation of ICT states.[76, 77]

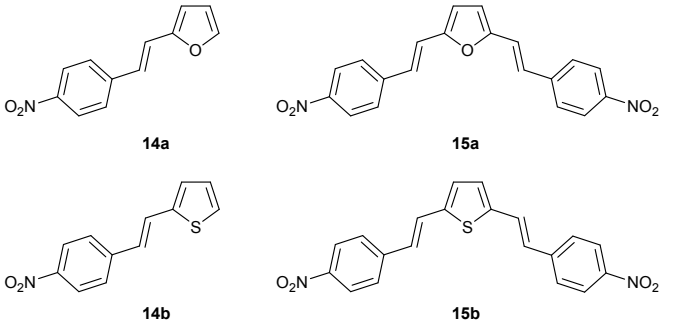

Fig. 10 The structure of heterocyclic analogues of nitrostilbenes **14a,b** and **15a,b**.

In nonpolar solvents the fluorescence is weak as the main relaxation pathway is the ISC. An increase in the solvent polarity turns on the ICT mechanism which is concurrent to the ISC thus strengthening the emission response (Table 6). Two-branched derivatives **15a,b** show much stronger emission than mono-branched **14a,b** even in non-polar solvents because the ISC pathway is slowed down due to the energy mismatch between S_1 and an accessible $^3(n,\pi^*)$ states.[76] A further increase in solvent polarity weakens the fluorescence, most probably because of lowering the energy of the non-planar CT states that decays *via* IC pathway.

Table 6 Photophysical properties of dyes **14a,b** and **15a,b**. Reproduced from Refs. [76, 77] with the permission. Copyright 2019 Elsevier.

	Solvent	λ_{abs} / nm	λ_{em} / nm	$\Delta\bar{\nu}_s$ / cm^{-1}	Φ_f (Φ_{ISC})
14a	Tol	376	471	5360	0.0005 (0.97)
	An	381	527	7270	0.09
	DCE	380	562	8520	0.30
	Ac	375	570	9120	0.34
	MeCN	374	597	9990	0.13 (0.51)
	DMF	383	594	9270	0.45
	DMSO	386	615	9650	0.30
14b	Tol	375	-	-	0.001 (0.24)
	An	379	519	7180	0.03
	DCE	378	552	8340	0.24
	Ac	373	556	8820	0.18
	MeCN	370	586	9960	0.15 (0.24)
	DMF	380	582	9130	0.40
	DMSO	384	601	9400	0.45

15a	Tol	441	521	3480	0.76 (0.11)
	An	450	568	4620	0.75
	DCE	450	624	6200	0.40
	Ac	444	630	6650	0.32
	MeCN	444	675	7710	0.10 (0.003)
	DMF	453	661	6950	0.18
	DMSO	458	688	7300	0.10
15b	Tol	434	517	3700	0.48 (0.45)
	An	444	549	4310	0.45
	DCE	443	603	5990	0.43
	Ac	437	605	6350	0.42
	MeCN	435	649	7580	0.21 (0.05)
	DMF	445	640	6850	0.34
	DMSO	453	661	6950	0.24

Konishi's group investigated the fluorescence properties of a series of quadrupolar thiophene derivatives bearing nitroaryl moieties (Fig. 11, Table 7).[75, 78] Compounds **16a-c** and **17a-c** show structural analogy with **13,** though they possess ethinyl linkers and thiophene moieties in lieu of vinyl chains and benzene rings. At the same time, one must remember that the sulfur atom of the thiophene ring can provide an additional energy dissipation channel through ISC, which should be considered.[79, 80] Within these two basic structures, the increase in the number of thiophene rings leads to small bathochromic shifts of the absorption that are typical for polyene chromophores. In terms of the fluorescence properties, all compounds experience a red-shift of the emission maxima with increasing solvent polarity, indicating the formation of CT states. Moreover, lengthening the thiophene oligomer increases the possible thorsional degrees of freedom. The latter is responsible for the weaker fluorescence response in comparison with compound **13**.

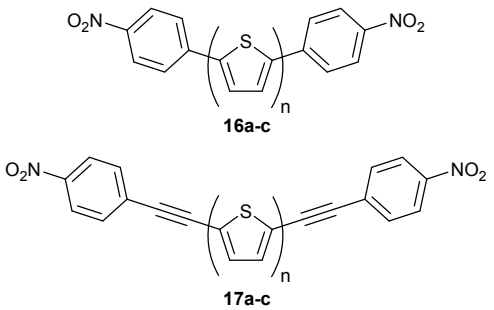

a: n=1; **b**: n=2; **c**: n=3

Fig. 11 Structures of dyes **16a-c** and **17a-c**.

Table 7 Photophysical properties of dyes **16a-c and 17a-c**. Reprinted with permission from [78] Copyright 2013 Elsevier.

cmpd	solvent	λ_{abs} / nm	λ_{em} / nm	$\Delta\bar{\nu}_s$ / cm^{-1}	Φ_f	τ_f / ns	$k_r \cdot 10^{-8}$ / s^{-1}	$k_{nr} \cdot 10^{-8}$ / s^{-1}
16a	PhMe[a]	386	498	5800	0.03	0.26	1.2	37.3
n = 1	CH_2Cl_2	388	501	5800	0.06	0.24	2.4	39.3
	DMSO	396	549	7000	0.40	1.44	2.8	4.2
16b	PhMe	420	497, 523	3700	0.22	0.51	4.2	15.3
n = 2	CH_2Cl_2	425	605	7000	0.40	1.64	2.5	3.6
	DMSO	436	667	7900	0.09	0.52	1.7	17.6
16c	PhMe	442	528, 559	3700	0.39	0.86	4.5	7.1
n = 3	THF	443	587	5500	0.25	0.86	2.9	8.8
	$CHCl_3$	444	667	7500	0.08	0.41	1.8	22.6
	CH_2Cl_2	446	684	7900	0.04	0.34	1.1	28.3
17a	THF	383	493	5800	0.01	0.28	0.4	35.3
n = 1	$CHCl_3$	390	538	7100	0.12	0.69	1.7	12.8
	CH_2Cl_2	389	553	7600	0.16	0.78	2.1	10.7
	DMF	386	578	8600	0.03	0.29	1.0	33.5
	DMSO	388	619	9600	0.02	0.21	0.9	46.8
17b	PhMe	413	486, 514	3600	0.34	0.33	10.2	20.2
n = 2	THF	411	556	6400	0.19	0.62	3.1	13.0
	$CHCl_3$	412	634	8500	0.04	0.18	2.4	50.3
	CH_2Cl_2	420	647	8400	0.01	0.22	0.4	45.1
17c	PhMe	436	518, 547	3600	0.44	0.33	13.4	16.9
n = 3	THF	436	609	6500	0.05	0.80	0.6	11.9

Sonoda *et. al.* presented[81, 82] a comprehensive study of the photophysics of nitro-substituted diphenyltrienes (Fig. 12) in a variety of solvents. Seminal works on the photophysics of (*E*,*E*,*E*)-1,6-diphenyl-1,3,5-hexatriene (DPH, **18a**) revealed the presence of two excited states close in energy, of which the S_2 state has ionic character and can be stabilized through effective modulation of the substitution pattern.[83, 84]

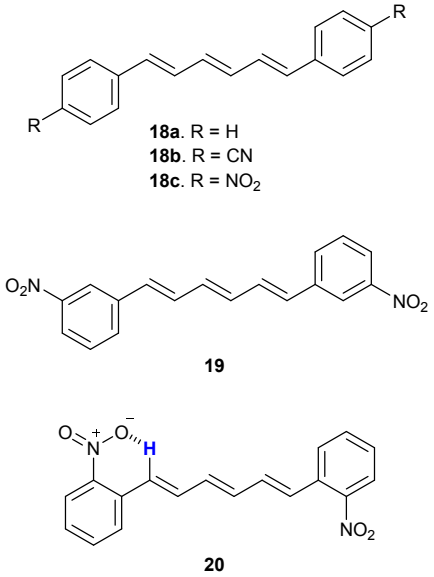

Fig. 12 Structures of dyes **18**-**20**.

Direct comparison of molecules bearing CN (**18b**) and NO_2 (**18c**) groups at the peripheries (Table 8) shows significant differences in their emission characteristics. Molecule **18c** exhibits strong solvatofluorochromic properties, while the positions of the emission maximum of **18b** do not depend on the solvent. This fact indicates a different nature of molecule **18c** in the ground and the singlet excited state, presumably resulting from the formation of a strongly polarized structure in more polar media. Theoretical calculations reveal that the

internal rotation around Ar-CH= and Ar-NO_2 single bonds occur almost freely, with low barrier heights. Hence, the stabilization of a TICT-type excited state in polar solvents cannot be ruled out in this case. Significant differences also arise from a comparison of fluorescence intensities, namely the value of Φ_f reaches its maximum for **18c** in dichloromethane (0.61), whereas for **18b** there is a gradual decrease from methylcyclohexane (0.80) to CH_3CN (0.032). Indisputably, the gradual decrease in emission efficiency for **18b** can be ascribed to stabilization of a CT* state with increasing polarity of the solvent, with the pure CT* state featuring an electron-density shift toward the cyanophenyl groups. The same holds true for molecule **18c**, namely the stabilization of the CT* state leads to a decrease in the value of Φ_f from CH_2Cl_2 to CH_3CN. The lower emission intensity determined for **18c** in less polar solvents (compared to CH_2Cl_2) is counterintuitive and might be related to the presence of an additional non-radiative decay channel connected with the NO_2 groups.

Table 8 The photophysical properties for **18b,c** and **19**. Reprinted with permission from Ref. [81,82] Copyright 2010 American Chemical Society and 2001 Royal Chemical Society.

cmpd	solvent	λ_{abs} / nm	λ_{em} / nm	$\Delta\bar{\nu}_s$ / cm^{-1}	Φ_f	τ_f / ns	$k_r \cdot 10^{-8}$ / s^{-1}	$k_{nr} \cdot 10^{-8}$ / s^{-1}
18c (18b)[b]	MCH[c]	395 (374)	460 (450)	3577 (4516)	0.002 (0.80)	<5 ps	---	---
	CCl_4	402 (378)	472 (452)	3690 (4331)	0.015 (---)	---	---	---
	PhMe	410 (380)	491 (452)	4023 (4192)	0.10 (0.88)	bi: 0.26 ns and 0.1 ns	?	?
	1,4-dioxane	408 (378)	493 (452)	4226 (4331)	0.28 (---)	---	---	---
	THF	411 (379)	508 (452)	4646 (4261)	0.53 (---)	---	---	---
	$CHCl_3$	414 (380)	542 (451)	5705 (4143)	0.60 (0.64)	mono: 1.9 ns (χ^2 = 10.9) bi: 2.0 ns (36%) and 0.05 ns (64%)	?	?
	CH_2Cl_2	415 (379)	549 (452)	5864 (4261)	0.61 (---)	---	---	---
	acetone	411 (375)	554 (452)	6280 (4543)	0.56 (---)	---	---	---
	DMF	422 (382)	578 (455)	6396 (4200)	0.44 (---)	---	---	---
	CH_3CN	410 (580)	7149 (4543)	7149 (4543)	0.30 (0.032)	2.2	1.4	3.2
19	MCH[c]	373, 355, 340	---[a]	---[a]	---[a]	---[a]	---[a]	---[a]
	CCl_4	379, 358, 342	482	7186	0.00042	0.72	0.0058	13.9
	PhMe	379, 360, 346	513	8285	0.0068	1.1	0.062	9.0
	1,4-dioxane	377, 357, 343	547	9729	0.011	1.7	0.065	5.8
	THF	377, 357, 343	574	10589	0.0052	1.3	0.040	7.6
	$CHCl_3$	378, 358, 343	---[a]	---[a]	---[a]	---[a]	---[a]	---[a]
	CH_2Cl_2	377, 357, 342	---[a]	---[a]	---[a]	---[a]	---[a]	---[a]
	acetone	374, 354, 338	---[a]	---[a]	---[a]	---[a]	---[a]	---[a]
	DMF	378, 359, 344	---[a]	---[a]	---[a]	---[a]	---[a]	---[a]
	CH_3CN	371, 352, 338	---[a]	---[a]	---[a]	---[a]	---[a]	---[a]

[a] No fluorescence detected. [b] Values in parentheses are for **18b**.[82] [c] Methylcyclohexane.

Solvent	λ_T / nm	τ_T / µs	Φ_T[a]
MCH	517	60	0.89
PhMe	546	75	0.31
$CHCl_3$	545	65	0.04
CH_3CN	552	80	<0.01

[a] +/- 15%.

Indeed the authors proved that extremely efficient triplet state formation is responsible for the lack of emission in non-polar methylcyclohexane (Table 8) and ISC becomes negligible in moderately polar $CHCl_3$ or polar CH_3CN. This trend is believed to remain essentially the same for the whole set of molecules described in this section. Thus, the majority of them reach their highest value of Φ_f in moderately polar solvents as a result of the interplay between three pathways of deactivation from different excited states: ^{1}LE, ^{1}CT and T_1. An analogue of **18c** bearing nitro groups at the *meta* positions (**19**) showed a similar trend in emission behavior (reaching a maximum Φ_f of 0.011 in dioxane), but the fluorescence quantum yields were significantly lower compared with those

determined for **18c**, which was ascribed to predominate formation of the ^{1}CT state. Molecule **20** was non-fluorescent in every solvent investigated. The authors suggest that excited-state intramolecular proton transfer (ESIPT) along the C-H···O type bond may be responsible for the lack of emission, as the distance between the hydrogen in the triene linker and the oxygen atoms is as low as 2.269-2.391 Å.

In contrast to strongly conjugated dyes containing double bonds between the nitro group(s) and a central unit (*vide supra*), the idea of controlling the photophysical properties *via* biaryl linkages may be of paramount importance in the strategy toward fluorescent nitroaromatics, as the existence of dihedral angles between subunits may allow for fine-tuning of the photophysical landscape. On the other hand, such an initial twist of a benzene ring may be the starting point for the formation of a TICT state.

Kotaka *et al*.[32] investigated a series of quadrupolar fluorene derivatives containing different functional groups at the peripheries connected *via* biphenyl-type linkages (Fig. 13). Molecules bearing CO_2Me (**21**), CN (**22**) are highly fluorescent in chloroform ($\Phi_f \geq 0.85$), while the value of Φ_f for **23** decorated with NO_2 groups drops down to 0.11, indicating an additional quenching mechanism due to the presence of NO_2 groups. Further spectroscopic studies revealed that the fluorescence response is strongly solvent dependent. Namely, **23** does not fluoresce in non-polar cyclohexane and toluene, but reaches the highest values of Φ_f in highly polar DMF and DMSO. The authors claimed that, in highly polar solvents, dye **23** fluoresces from the TICT state as the fluorescence maximum of **23** in DMSO was red-shifted by 51 nm relative to the maximum measured in chloroform. No evidence, however, supports this claim (Table 9). Moreover, in the light of other findings related to nitroaromatics it is highly unlikely that a TICT state would be fluorescent. The lack of emission in both cyclohexane and toluene may be associated with efficient triplet formation; however, the authors did not report any phosphorescence studies.

In contrast to **23**, dye **24**[85] fluoresces predominately in solvents of low polarity, reaching the highest value of Φ_f in toluene (0.37) (Figs. 13-14). The larger size of the central core and hence stronger electron-donating ability may be the reason behind the lack of fluorescence in dichloromethane, as **24** may exhibit a higher tendency for the formation of a TICT state in polar solvents, compared to **23**. Additionally, both **23** and **24** show strong solvatochromic behavior.

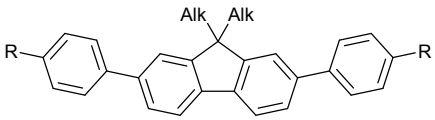

Alk = *n*-C_8H_{17}

21. R = CO_2Me; **22**. R = CN
23. R = NO_2

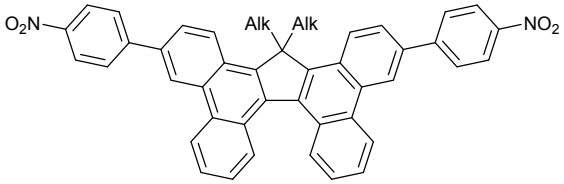

24. Alk = *n*-C_5H_{11}

Fig. 13 Structures of dyes **21**-**24**.

Table 9 Spectroscopic properties for compounds **23** and **24** in different solvents. Copyright 2021 Wiley. Used with permission from Ref. [85]

		23							24			
	$E_T(30)$	λ_{abs} / nm	λ_{em} / nm	$\Delta\bar{\nu}_s$ / cm^{-1}	Φ_f	τ_f / ns	$k_r \cdot 10^{-8}$ / s^{-1}	$k_{nr} \cdot 10^{-8}$ / s^{-1}	λ_{abs} /nm	λ_{em} /nm	$\Delta\bar{\nu}_s$ / cm^{-1}	Φ_f
C_6H_{12}	30.9	357	Nd[a]	---	---	---	---	---	427	458	1600	Nd[b]
Toluene	33.9	365	Nd[a]	---	---	---	---	---	422	485	3100	0.37
Et_2O	34.5	---	---	---	---	---	---	---	417	497	3900	Nd[b]
THF	37.4	---	---	---	---	---	---	---	425	541	5000	0.18
DME		---	---	---	---	---	---	---	422	546	5400	0.05
$CHCl_3$	39.1	373	538	8200	0.11	1.18			428	554	5300	0.01
CH_2Cl_2	40.7	---	---	---	---	---	---	---	430	Nd[a]	---	---
acetone	45.6	---	---	---	---	---	---	---	422	Nd[a]	---	---
DMF	45.4	380	569	8700	0.31	1.92	1.6	3.6	427	Nd[a]	---	---
DMSO	51.9	382	589	9200	0.28	1.82	1.5	4.0	429	Nd[a]	---	---

a Not detected. b Not determined due to low solubility of a dye in a given solvent.

Summing up, among nitro-aromatics **1-18**, **23** and **24** the general tendency is that, in non-polar solvents, the fluorescence is rather low or moderate because the emission is concurrent with ISC. Increasing the solvent polarity lowers the energy of the ^{1}LE* state due to a partial charge separation or forms a planar ^{1}CT* state that makes emission the main deactivation pathway. In solvents of intermediate polarity the fluorescence reaches its maximum values and in polar solvents it weakens and essentially disappears due to formation of a CT states with a twisted geometry. In the exceptional case of dyes **12** and **13**, the quadrupolar or quasi-quadrupolar geometry somehow suppresses formation of a TICT state, enabling the steady increase in the fluorescence up to solvents as polar as DMF and DMSO.

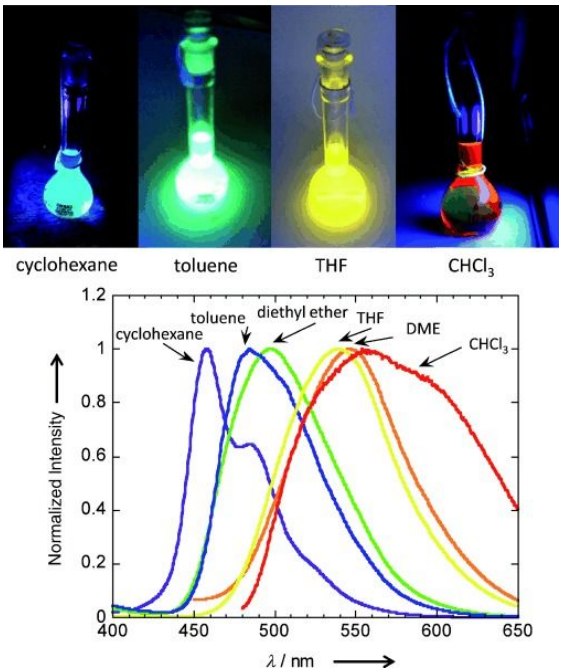

Fig. 14 Fluorescence color (photographs) and normalized fluorescence spectra of **24** in various solvents. Copyright 2021 Wiley. Used with permission from Ref. [85]

Suppressing intersystem crossing in non-polar solvents

Nitro group directly linked to the main core to form small dipolar dyes

For the most of the remaining cases of nitroaromatics, the fluorescence is the strongest in non-polar solvents, and steadily or rapidly decreases as the medium polarity increases. Thus corresponds, in most cases where details are known, to the transition from a planar CT state to a TICT state. There are rather spectacular cases of small dipolar nitro-fluorophores possessing such characteristics.

Nitrobenzene is the smallest nitroaromatic compound and it is not fluorescent. Its relative simplicity, however, has attracted some attention to it and its derivatives for studies aiming at deciphering the excited-state dynamics and fluorescence properties of nitroaromatics.[86, 87] Enhancing the CT character of nitrobenzene by converting it to nitroaniline, actually, leads to some weak but detectable fluorescence.[87]

At cryogenic temperatures, i.e., around 100 K, nitroanilines **25a-c** (Fig. 15) exhibit both phosphorescence and fluorescence. While **25a** and **25b** yield strong phosphorescence and weak fluorescence, the conformationally locked **25b** produces strong fluorescence and weak phosphorescence.[87] That is, suppressing the formation of TICT states in nitroanilines, as in **25b**, enhances the preference for $S_1 \rightarrow S_0$ radiative deactivation over ISC. Furthermore, even **25c**, which assumes sterically forced twisted geometry, shows detectable fluorescence.

At room temperature neither of the nitroanilines yield any detectable emission. It is essential to lower the temperature under about 150 K for these compounds to fluoresce.[87] A temperature decrease drastically enhances the fluorescence quantum yields of all three nitroanilines (Fig. 15) reaching maximum values around 100 K. With its amine locked in a planar geometry, **25b** cannot form a TICT state. Nevertheless, **25b** shows the same temperature-dependence trend as **25a** and **25c**. Thus, the reported temperature dependence of the fluorescence efficiency most likely does not originate from the thermally activated formation of TICT states which are dark.[87]

Nitronaphthalenes are also among the smallest nitroaromatics that show record-fast subpicosecond rates of ISC.[88] Therefore, making nitronaphthalenes fluoresce is as challenging as it is important for developing paradigms for attaining emissive electron-deficient chromophores. Introducing electron-donating substituent to the para position of the nitro group does not yield much improvement of the fluorescent properties of 1-nitronaphthalene.[89] In contrast, shifting the electron-donating substituent to the other ring of the naphthalene, i.e., the ring without the nitro group, makes a huge difference in the excited-state dynamics. Specifically, the lifetimes of the S_1 states of **26a** and **26b** (Fig. 15) in certain solvents are almost four orders of magnitude longer than the lifetime of the parent 1-nitronaphthalene.[8]

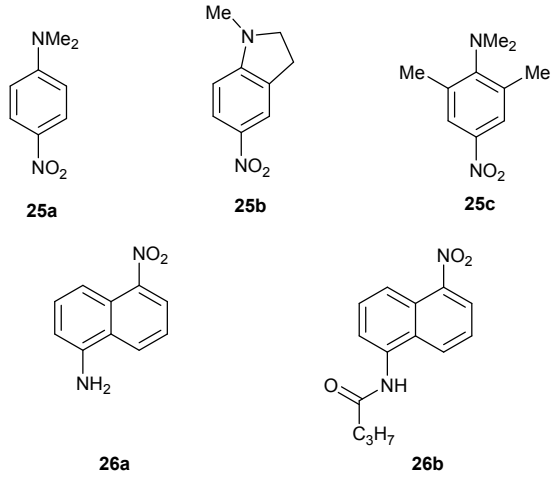

Fig. 15 The structures of nitrobenzenes **25a-c** and nitronaphthalenes **26a,b**.

The nitronaphthalenes **26a** and **26b** have a propensity for aggregation even at μM concentrations. Nevertheless, their photophysics shows the two different polarity-dependence trends, observed for the known fluorescent nitro organic compounds. The S_1 lifetime, τ, of **26a** in toluene is about 0.7 ns and its fluorescence quantum yield, ϕ_f, is about 0.01. An increase in solvent polarity, substantially quenches the fluorescence of **26a** without noticeable production triplets. For **26a** in acetonitrile, $\tau \approx 3$ ps and $\phi_f \approx 3\times10^{-5}$ and this noticeable increase in the non-radiative rates of deactivation does not involve ISC.[8]

Lowering the electron-donating strength of the ancillary substituent, i.e., **26b** vs. **26a** (Fig. 15), completely shifts the photophysical paradigm of polarity dependence. In toluene, **26b** manifests relatively weak fluorescence, i.e., $\tau \approx 0.3$ ns and $\phi_f \approx 5\times10^{-4}$. An increase in medium polarity enhances its

fluorescence, i.e., τ and ϕ_f of **26b** in dichloromethane are 0.7 ns and 2×10^{-3}, respectively. A further increase in medium polarity, however, quenches the fluorescence of **26b**, i.e., for acetonitrile, $\tau \approx 0.2$ ns and $\phi_f \approx 4\times10^{-4}$.[8] TAS reveals that unlike **26a**, triplet formation prevails the decay pathways of photoexcited of **26b** in non-polar and moderately polar media.[8] This behavior of **26b** is consistent with the trends of solvent effects on the fluorescence of nitroaromatics that we discuss in the previous section.

These examples of small nitroaromatics with electron-donating substituents (Fig. 15) show the importance of balancing the CT character of their singlet excited states for making them fluorescent. Fusing the benzene ring of 4-nitroanliline with a 2-oxa-1,3-diazole heterocycle (Fig. 16), however, produces strongly fluorescent chromophores that proved to be a practical breakthrough for biochemistry, cell biology and biophotonics.[13,91]

As early as 1968, Ghosh and Whitehouse synthesized 4-nitrobenzo-2-oxa-1,3-diazole (NBD) derivatives as antileukemia agents.[13] Surprisingly, despite the presence of a nitro group, some 7-amino NBD derivatives featured strong fluorescence properties[90] (Scheme 1).

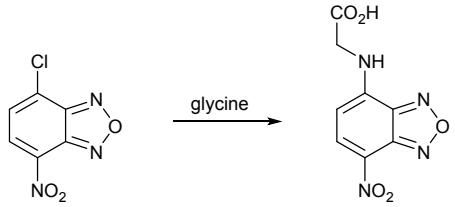

27 nonfluorescent **28** highly fluorescent

Scheme 1 Transformation of 4-chloro-7-nitrobenzooxadiazole **27** into the fluorescent derivative **28**.

Due to its strong emission response and a low molecular weight, NBD has become a convenient fluorescent labelling scaffold,[91] and the influence of wide variety of electron-donor substituents has been studied.[92] More recently, analysis of NBDs *via* both spectroscopy and computational studies has revealed that the structure and function of the NBD chromophore is more complex that it seemed at first glance. The benzo-2-oxa-1,3-diazole (BD) system not only acts as a spacer, but it provides an electronic effect on the charge distribution, making NBDs efficient fluorophores. Both the nitro group and the heterocyclic nitrogen atoms act as electron-withdrawing sites. For this reason, three features that affect both the absorption and fluorescence properties must be considered.[93, 94] Moreover, modification at the 2-position with heteroatoms from group 16 other than oxygen does not significantly affect the chromophore character.[93, 95] To study the influence of nitrogen atoms, the NBD chromophore was compared with the analogous structure based on an electron-rich core (Fig. 16).[93, 94]

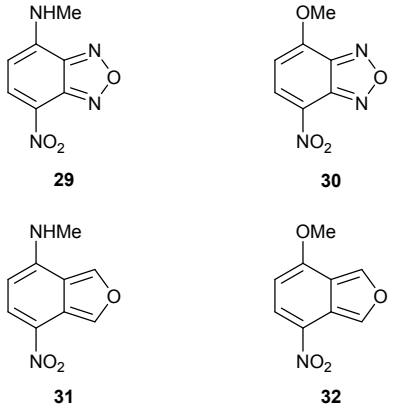

Fig. 16 The structures of nitrobenzo-2-oxa-1,3-diazoles **29** and **30** and the corresponding isobenzofuran derivatives **31** and **32**.

Computational studies show that the fluorescence properties of NBDs **29**, **30** and the nitro-isobenzofurans (IBF) **31**, **32** are connected by the formation of CT states, where the natures of the electron-donor groups and the heterocyclic site play a crucial role. In fact, the nitrogen atoms in the NBD scaffold introduce electron-acceptor characteristics, and in the CT state the electron density is partially shifted towards the furazane moiety. Concerning electron-donating substituents, only strongly electron-rich groups can support efficient charge transfer. In nonpolar cyclohexane, compound **29** exhibits a moderate fluorescence response. As the polarity is gradually increased, a growth in the fluorescence efficiency is observed. While the fluorescence is strong in the majority of solvents, it slightly decreases in acetonitrile and alcohols, and significantly dims in water (Table 10). [93, 96] Conversely, the NBD with a methoxy group, **30,** shows very weak fluorescence.

Table 10 Photophysical properties of strongly polarized dyes **27**-**30** possessing NBD and IBF cores. Reprinted with permission from *Org. Lett.*, 2019, **21**, 3817-3821. Copyright 2019 American Chemical Society.

solvent	$E_T(30)$	**29**			**30**			**31**			**32**		
		λ_{abs} / nm	λ_{em} / nm	Φ_f	λ_{abs} / nm	λ_{em} / nm	Φ_f	λ_{abs} / nm	λ_{em} / nm	Φ_f	λ_{abs} / nm	λ_{em} / nm	Φ_f
C_6H_{12}		425	499	0.16									
toluene	33.9	442	508	0.49 (0.44)	368	405	0.019	469	495	0.18 (0.17)	423	505	0.22 (0.085)
dioxane	36	448	516	0.71	359	406	0.027	471	501	0.128	425	519	0.31
THF	37.4	454	520	0.71	366	405	0.008	477	502	0.047	423	515	0.26
DCM	40.7	449	514	0.55	370	406	0.023	475	518	0.030	433	529	0.12
CH_3CN	45.6	458	527	0.48	369	400	0.010	482	520	0.017	431	541	0.004
methanol	55.4	461	532	0.23	357	402	0.005	485	536	0.008	429	569	0.004
water	63.1	478	552	0.013	381	ND	ND	512	548	0.001	451	607	0.001

The Φ_f values in parentheses were determined for air equilibrium solutions.

On the other hand, in the IBF chromophores the furan moiety acts as an electron-donor and the electron distribution in the excited state is completely different.[94] In contrast to fluorescent NBD **29**, the IBF analogue **31** shows a much weaker fluorescence response, whereas the methoxy derivative **30** shows intense fluorescence (Table 10). Both spectroscopic and computational studies suggest that, for NBD, the ISC relaxation pathway is not typical, even in nonpolar solvents.[93]

Saha and co-workers developed and systematically studied a series of NBDs containing free and substituted amino groups with respect to their fluorescence efficiency.[97]

NBD derivatives exhibit strong fluorescence in nonpolar media, while an increase in the solvent polarity causes a gradual decrease in fluorescence. The character of amino substituents affects the conjugation that in turn governs how prone NDBs are to formation of a planar CT state. Lengthening the linear alkyl substituents on the amino group (**33**-**35**) tends to decrease the fluorescence efficiency as the possibility of radiationless deactivation of the excited state becomes more preferable. For the same reason, NBDs **36** and **37** with the amino group in strained rings, are less sensitive to solvent polarity and exhibit strong fluorescence in nonpolar solvents and meaningful fluorescence levels in solvents as polar as acetonitrile and methanol. This is less evident for **38,** which contains the amine nitrogen in a less strained ring (Fig. 17, Table 11).

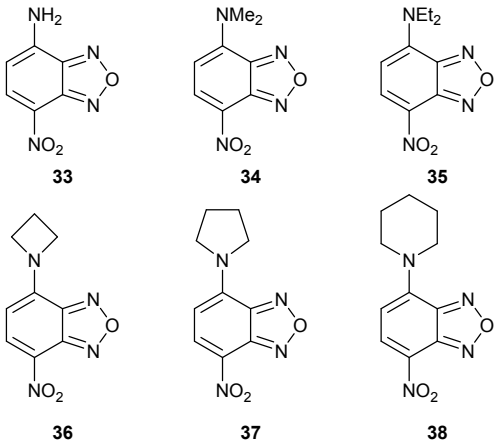

Fig. 17 The structures of nitro-NBDs **33**-**38** possessing various amino groups.

Table 11 The photophysical properties of nitro-NBDs **31**-**36** possessing various amino groups. Adapted with permission from *J. Phys. Chem. A*, 1998, **102**, 7903-7912. Copyright 1998 American Chemical Society.

solvent	$E_T(30)$	**33**			**34**			**35**			**36**			**37**			**38**		
		λ_{abs} / nm	λ_{em} / nm	Φ_f	λ_{abs} / nm	λ_{em} / nm	Φ_f	λ_{abs} / nm	λ_{em} / nm	Φ_f	λ_{abs} / nm	λ_{em} / nm	Φ_f	λ_{abs} / nm	λ_{em} / nm	Φ_f	λ_{abs} / nm	λ_{em} / nm	Φ_f
toluene	33.9	423	504	0.13	461	519	0.52	468	522	0.28	467	524	0.49	467	517	0.49	468	528	0.48
dioxane	36	436	515	0.46	465	527	0.15	470	525	0.07	468	530	0.57	468	523	0.41	470	533	0.12
THF	37.4	445	517	0.79	468	527	0.14	477	526	0.02	472	530	0.59	472	524	0.22	474	536	0.03
DCM	40.7	429	504	0.45	473	526	0.16	479	529	0.02	477	530	0.51	478	525	0.27	482	539	0.03
ACN	45.6	445	521	0.57	478	539	0.02	485	543	0.01	483	542	0.44	484	537	0.11	487	551	0.01
methanol	55.4				477	541	0.02	484	551	0.01	481	545	0.19	481	543	0.06	484	551	0.01
water	63.1				497	558	0.01	505	562	0.004	499	572	0.02	500	560	0.01	508	571	0.002

The approach to modulate the strength of NBD fluorescence employs photoinduced electron transfer (PET),[98, 99] where the energy level of the HOMO orbitals of n-donors governs the fluorescence quenching in **39a-i** (Scheme 2, Table 12).[100] The fluorescence efficiency depends on both the electron-donor strength and the medium polarity. The HOMO level of the isolated electron donors (*e.g.,* NMe_2 or $MeNH_2$) correlates well with the fluorescence decrease in comparison with unsubstituted **29** (Table 10). In the case of compounds **40** and **42,** the oxidation of the phosphine center inhibits PET processes, resulting in switching on of the emission pathway (Scheme 2, Table 12).[101]

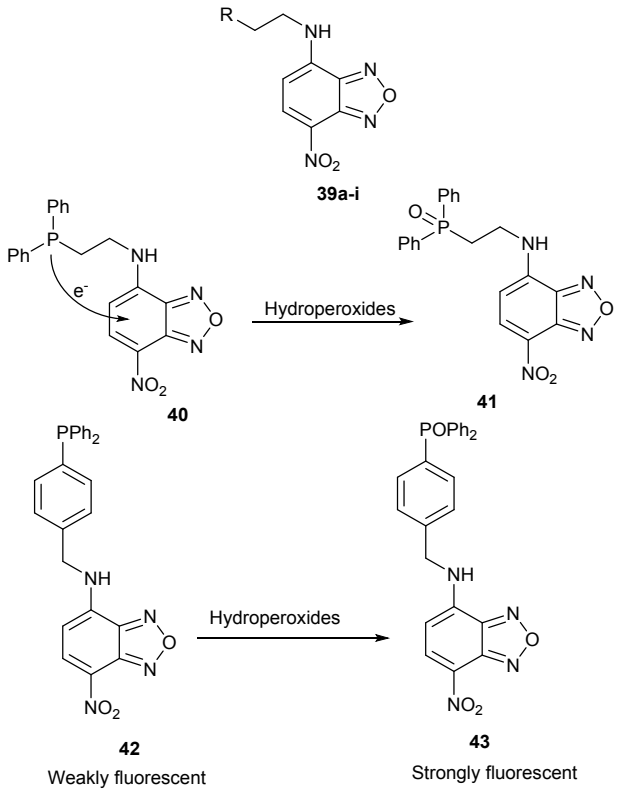

Scheme 2 Transformation of **40** and **42** into fluorescent derivatives **41** and **43**.

Table 12 The photophysical properties of dyes **39a-i** and **40-43**. Adapted with permission from *Anal. Chem.*, 2002, **74**, 4089-4096 and *Org. Lett.*, 2003, **5**, 1459-1461. Copyright 2002, 2003 American Chemical Society.

no.	R	C_6H_6				CH_3CN				methanol			
		λ_{abs} / nm	$\varepsilon \cdot 10^{-4}$ / $M^{-1}cm^{-1}$	λ_{em} / nm	Φ_f	λ_{abs} / nm	$\varepsilon \cdot 10^{-4}$ / $M^{-1}cm^{-1}$	λ_{em} / nm	Φ_f	λ_{abs} / nm	$\varepsilon \cdot 10^{-4}$/ $M^{-1}cm^{-1}$	λ_{em} / nm	Φ_f
39a	NMe_2	451	1.69	511	0.0091	462	2.06	525	0.00038	461	2.00	522	0.0051
39b	NEt_2	453	1.76	509	0.0084	464	2.09	526	0.00017	464	2.04	520	0.0089
39c	NHMe	451	1.56	512	0.087	462	1.85	524	0.0018	458	1.69	522	0.046
39d	NH_2	453	1.75	512	0.23	461	2.06	536	0.014	458	2.02	524	0.078
39e	NHAc	453	1.50	511	0.26	461	1.85	525	0.30	461	1.93	528	0.17
39f	NMeAc	450	1.51	510	0.43	461	2.13	526	0.32	460	1.78	528	0.16
39g	OH	452	1.59	510	0.33	460	1.92	528	0.29	464	2.17	531	0.14
39h	OMe	449	1.55	510	0.37	459	1.95	525	0.30	463	1.97	531	0.14
39i	OAc	446	1.57	505	0.31	457	1.93	523	0.32	456	1.93	527	0.17
40		451 [a]		508	0.051	461 [a]		522	0.014	466 [a]		527	0.0073
41		449 [a]		505	0.42	458 [a]		520	0.44	459 [a]		525	0.21
42		446 [a]		507	0.30	456 [a]		521	0.050	461 [a]		527	0.027
43		444 [a]		504	0.22	454 [a]		520	0.36	457 [a]		526	0.19

[a] - Excitation wavelength

Table 13 The experimental and calculated spectroscopic properties of the phenothiazines **44**-**47**. Copyright 2020 Wiley. Used with permission from Ref. [25]

	λ_{abs} / nm		λ_{em} / nm		$\Delta\bar{\nu}_s$ / cm^{-1}		Φ_f / τ_f [ns] k_r [s^{-1}]/k_{nr} [s^{-1}]		
	Exp[a]	Calcd (*f*)	Exp[a]	Calcd (*f*)	Exp[a]	Calcd	C_6H_{12}	Toluene	CH_2Cl_2
44	318	303 (0.0007)	433	420 (0.0080)	8400	9200	0.0016/0.74 $2.16\times10^6/1.35\times10^9$	0.0024/0.86 $2.80\times10^6/1.16\times10^9$	0.0022/0.81 $2.73\times10^6/1.24\times10^9$
45	331	323 (0.0741)	457	443 (0.0559)	8300	8400	0.066/5.07 $1.31\times10^7/1.84\times10^8$	0.11/5.52 $2.13\times10^7/1.60\times10^8$	0.11/5.99 $1.81\times10^7/1.49\times10^8$

	λ_{abs} / nm		λ_{em} / nm		$\Delta\bar{\nu}_s$ / cm^{-1}		Φ_f / τ_f [ns] k_r [s^{-1}]/k_{nr} [s^{-1}]		
	Exp[a]	Calcd (*f*)	Exp[a]	Calcd (*f*)	Exp[a]	Calcd	C_6H_{12}	Toluene	CH_2Cl_2
46	376	340 (0.1248)	458	461 (0.0988)	4800	7700	0.44/8.22 5.30×10^7/6.87×10^7	0.46/8.47 5.45×10^7/6.36×10^7	0.41/7.98 5.13×10^7/7.39×10^7
47	408	362 (0.1873)	522	496 (0.1694)	5400	7500	1.00/7.63 1.31×10^8/–	0.29/2.76 1.06×10^8/2.57×10^8	0.0054/0.24 2.29×10^7/4.22×10^9

[a] – measured in C_6H_{12}.

The addition of a nitro group often gives rise to formation of CT states that promote the relaxation of the excited state of the molecule *via* radiationless pathways. In some cases, however, a charge redistribution towards a CT state tends to disfavor non-radiative relaxation mechanisms in favor of the fluorescence channel. Unsubstituted phenothiazine **44** shows no significant fluorescence response due to the presence of the sulfur atom. The lowest singlet excited state has an nπ* character, favoring non-radiative pathways of deactivation. In phenothiazines **45**-**47** (Fig. 18, Table 13), electron-withdrawing groups (EWG) remove the electron density from the sulfur atom, decrease the LUMO energy, make the lowest singlet excited state a ππ* state and turn on the fluorescence.[25] Among typical EWGs, the nitro group demonstrates the strongest effect. In the case of 3-nitrophenothiazine **47**, this effect of the electron-withdrawing nitro group enhances the fluorescence efficiency to as high as unity for cyclohexane. Weaker EWGs also turn on the fluorescence response, though less efficiently. As the CT states are sensitive to solvent polarity, the fluorescence spectra measured in toluene and dichloromethane show a gradual bathochromic shift of the fluorescence bands, along with a decrease in the fluorescence efficiency, that indicates the formation of a CT state (Fig. 19). The character of the solvatofluorochromism is commensurate for all EWGs, showing different red shifts and effects on the fluorescence efficiency that depend on the electron-acceptor strength.

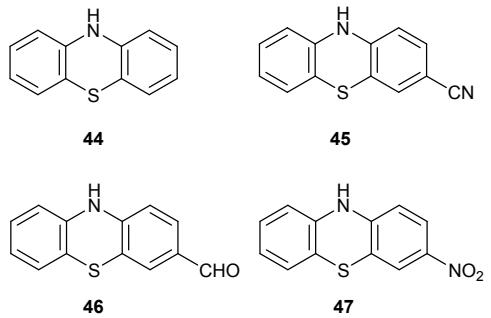

44 **45** **46** **47**

Fig. 18 Structures of phenothiazine derivatives **44**-**47**.

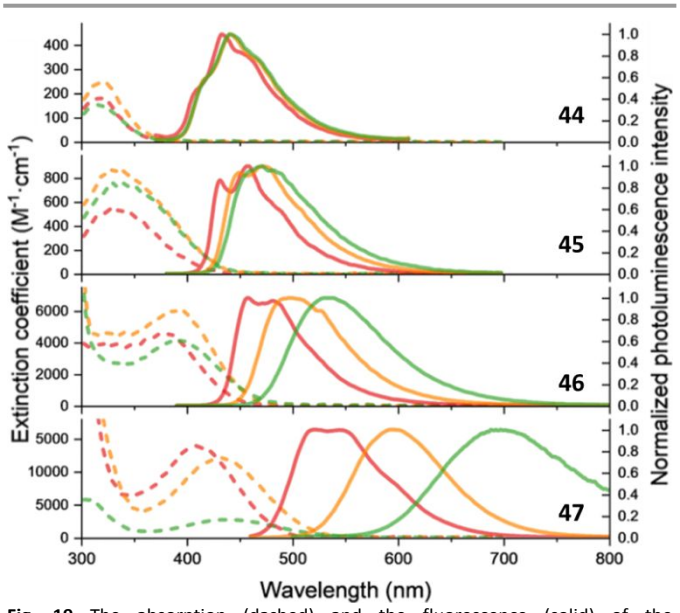

Fig. 19 The absorption (dashed) and the fluorescence (solid) of the phenothiazines **44**-**47**. Copyright 2020 Wiley. Used with permission from Ref. [25]

Nitro groups introduced as nitroaryl substituents to form dipolar and quadrupolar dyes

Interestingly, the same interplay between planar and twisted charge-transfer states plays a role in larger systems possessing either dipolar or quadrupolar architecture.

The dithiophene chromophores substituted with nitro and amino groups are another example of fluorescent nitro derivatives (Fig. 20).[102] Among the nitro-dithophenes **48**-**50** only compound **48** shows efficient fluorescence, while chromophores **49** and **50** with nitro groups at the *ortho*-position relative to the adjacent thiophene ring exhibit weak fluorescence, similar to dinitrostilbene **49**, where the fluorescence is quenched *via* a non-planar ICT state.[66] Dye **48** shows very strong emission response in nonpolar solvents, but upon increasing the polarity, the fluorescence maximum exhibits a small red-shift, accompanying slight dimming of the emission (Table 14, Fig. 21). In comparison with other fluorescent nitroaromatics, the emission response of **48** is less susceptible to the solvent polarity as it is still significant in acetonitrile (Φ_f=0.34) and efficiently quenched only in highly polar DMSO and protic solvents.

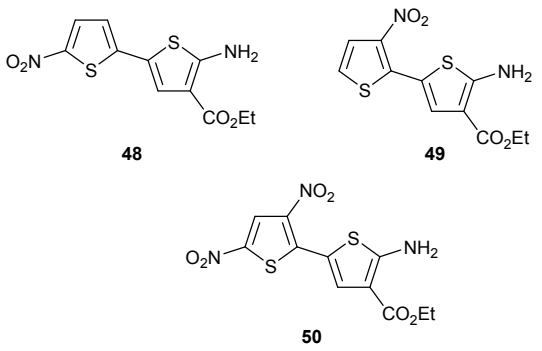

Fig. 20 Structures of nitro-thienylthiophenes **48-50.**

Because TAS experiments for **48-50** did not produce detectable transients and Lippert-Mataga functions gave poor correlations, the conclusions about the properties of these three dyes were drawn mostly from steady-state spectroscopic data and information about analogous dithiophenes.[102] For chromophore **48**, the relaxed and solvated ^{1}ICT* state is partially planar[103,104] and undergoes a relatively fast radiative deactivation showing strong emission (Table 13). An increase in the solvent polarity leads to an additional stabilization of the ^{1}ICT* state, resulting in a red-shift of the emission bands. Concerning the effects of highly polar solvents, the authors claim that the non-radiation deactivation results mainly from narrowing the singlet–triplet energy gap, which favors ISC to the triplet manifold, though without experimental data that would confirm this suggestion.[102] On the other hand, the data reported for nitrostilbenes and related compounds rationalize the fluorescence quenching under similar conditions in terms of the formation of a charge transfer state with the twisted geometry, resulting in efficient IC *via* bond rotation.[63-67, 69, 71] In the light of these publications, the hypothesis of ISC dominating the non-radiative deactivation pathways in polar media is rather dubious.

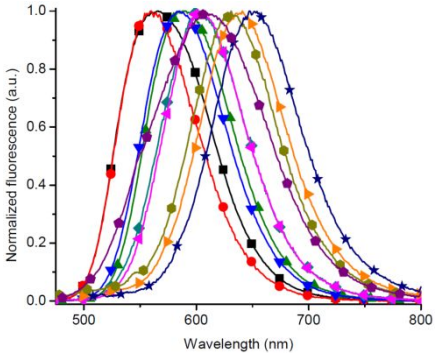

Fig. 21 Normalized fluorescence of **48** in toluene (■), diethyl ether (●), THF (▲), ethyl acetate (▼), $CHCl_3$ (♦), CH_2Cl_2 (◀), DMF (▶) CH_3CN (⬢), DMSO (★) and ethanol (⬟). Reproduced from Ref. [102]

Table 14 Photophysical properties of compounds **48-50** in different solvents. Reproduced from Ref. [102]

			48				49				50			
	Δf	$E_T(30)$	λ_{abs} /nm	λ_{em} /nm	$\Delta\bar{\nu}_s$ / cm^{-1}	Φ_f	λ_{abs} /nm	λ_{em} /nm	$\Delta\bar{\nu}_s$ / cm^{-1}	Φ_f	λ_{abs} /nm	λ_{em} /nm	$\Delta\bar{\nu}_s$ / cm^{-1}	Φ_f
Toluene	0.013	33.9	455	566	4310	0.97	449	564	4541	0.04	491	566	2699	0.04
Et_2O	0.167	34.5	455	560	4121	0.92	450	585	5128	0.02	496	567	2525	0.01
THF	0.210	37.4	471	589	4253	0.85	457	592	4990	0.02	503	590	2932	~0
EtOAc	0.200	38.1	463	584	4475	0.79	453	597	5325	0.02	496	585	3067	0.02
$CHCl_3$	0.149	39.1	463	604	5042	0.62	453	606	5573	0.02	493	595	3477	0.01
CH_2Cl_2	0.218	40.7	494	600	5170	0.76	450	615	5960	0.03	494	600	3575	0.02
CH_3CN	0.305	45.6	469	631	5474	0.34	454	630	6153	~0	493	626	4310	~0
DMSO	0.263	45.4	499	652	4703	—	478	644	5393	0.01	523	645	3617	0.01
EtOH	0.290	51.9	472	608	4739	~0	454	608	5579	0.02	503	598	3158	~0
MeOH	0.309	55.4	471	617	5024	~0	456	603	5346	0.02	496	583	3009	0.01

Absolute fluorescence quantum yields determined with an integrating sphere

Among known heteropentalenes, the pyrrolo[3,2-*b*]pyrrole[105, 106] core (PP) constitutes the most electron-rich scaffold. We have recently demonstrated that a simple pyrrolo[3,2-*b*]pyrrole-based chromophore **51** bearing two peripheral 4-nitrophenyl groups (Fig. 22) fluoresces almost quantitatively in cyclohexane, while the fluorescence response sharply decreases upon increasing the medium polarity and eventually vanishes in relatively polar solvents, such as dichloromethane (Table 15).[33, 107-109]

Both computational studies and TAS experiments on **51** revealed that, after the excitation and the solute-solvent interaction, the chromophore experiences a fast transition from ^{1}LE* to a CT state with reduced dihedral angles between the terminal nitroaryl moieties and the central framework relative to the ground state. Thus, in the first CT state both nitro groups are more strongly conjugated with the central framework than in the ground state.[20, 110, 111] TAS shows that, in the nonpolar solvent cyclohexane, ISC is slowed down in favor of the fluorescence relaxation pathway. An increase in solvent polarity leads to a second CT state with one nitroaryl substituent twisted in relation to the rest of the chromophore, causing fluorescence quenching. This excited-state symmetry breaking was studied within a similar family of molecules bearing 4-cyanophenyl moieties,[112] and proves to be characteristic for the excited-state dynamics of tetraarylpyrrolo[3,2-*b*]pyrroles (TAPPs) with nitro groups.[20,

[110, 111] Thus, an approach to the design of dinitro- TAPPs should be based on the balance between the donor-acceptor strength of the chromophore counterparts and an enforcement of a planar geometry of the chromophore.

The presence of substituents governing the chromophore geometry indeed affects the spectroscopic properties of dinitro-TAPP. The analysis of pyrrolo[3,2-*b*]pyrroles with relatively planar geometries (**51**-**53**), rigidified structures (**54**), and enforced non-planar conformations **55**-**57** shows that the planarity distortion causes a partial loss of conjugation (Fig. 22, Table 15). TAPP **55**, retaining the same conjugation length as **51**, shows in contrast weak blue-shifted absorption. Among these examples, computational data for **55** show the largest dihedral angle between the terminal nitroaryls and the central core, i.e., 66°. Due to the presence of four methyl groups, the π-system is far from planarized, compromizing the overlaps between the NTOs involved in the long-wavelength optical absorption and emission transitions between the S_0 and S_1 states. Thus, **55** shows considerably weaker absorption and fluorescence response than **51**.[111] As the planarity of the excited state plays a crucial role in the fluorescence efficiency, even small moieties which inhibit efficient conjugation can cause a fluorescence decrease. Moreover, a subtle increase in the media polarity can quench the fluorescence due to the stabilization of the twisted CT state. The presence of substituents inducing a minor planarity distortion, such as in **56**, **57** (in comparison with **55**), result in somewhat blue-shifted absorption and weaker fluorescence efficiency in comparison with **51**.[110, 111]

Formation of a CT state with a twisted geometry tends to be a common reason for fluorescence quenching. Nitro groups at the *ortho*-position in dye **58** prevent the chromophore from adopting a planar structure (similar to **49**, **50**).[103] On the other hand, nitrophenyl moieties bound through the central nitrogen atoms in **59** are formally "decoupled" from the central chromophore and thus a planar CT state cannot form. Compounds **58** and **59** show no fluorescence response. Despite the similarity in the fluorescence properties (or the lack of such) of **58** and **59**, the reasons for the undetectable emission of these two compounds are not quite the same. The formation of TICT states with negligible or no overlap between their NTOs for radiative deactivation, indeed, makes the rates of fluorescence decay considerably smaller than the rates of the competing non-radiative processes. In **58**, however, placing the nitro group at the *ortho* position to the chromophore core enhances the SOC and the ISC rates by orders of magnitude, which further precludes any detectable fluorescence.[20]

Compounds **52**, **53** are heterocyclic analogues of **51** possessing 5-membered heterocycles instead of benzene rings. The former show smaller steric hindrance that may, in theory, permit better planarity. In fact **52**, **53** exhibit somewhat weak fluorescence, probably because furan and especially thiophene moieties act as ancillary electron donors. In contrast, when two carbon bridges permit the planarity of the terminal nitro aryl substituents (**54**), the TAPP chromophore shows enhanced absorption in the same spectral range as **51**. The fluorescence of **54** is also polarity sensitive and exhibits a red-shift upon increasing solvent polarity. The extent of this effect, however, diminishes quite smoothly as the bridging inhibits the formation of a fully twisted CT state (Table 15).[110] The magnitude of charge transfer from the central core towards the terminal nitro-aryl acceptors correlates well with dihedral angles. TAPP **52** has a dihedral angle as small as 6.7° and the smallest extent of charge separation in its CT state, while **53** forms a conformer with the largest angle (of 66°) with the most pronounced CT character among such compounds.[110, 111]

Highly polar media tend to stabilize CT states with distorted planarity, which results in solvatochromism and fluorescence quenching.[20] Another specific case is the TAPP **60** bearing a pure dipolar structure as one of the nitro groups is replaced with a morpholine moiety. For **60**, computational studies show almost no change in the dihedral angle upon photoexcitation. This derivative shows no fluorescence response in any solvents.[110]

The modification of the electron-donating ability of the central framework and terminal moieties can affect the charge distribution and affect spectroscopic properties. Introducing electron-acceptor groups in lieu of alkyl groups on *N*-aryl substituents (**61**) partially withdraws the electron density from the central framework relative to the model **51**. This modification results in only a small blue-shift of the absorption maximum (ca. 27 nm), without a loss of fluorescence efficiency because the pyrrole nitrogen atoms tend to diminish the electronic coupling across them. On the other hand, the addition of electron-acceptor moieties at the positions 3 and 6 (**62**, **63**) causes a significant withdrawal of the electron density from the pyrrolo[3,2-*b*]pyrrole system, resulting in a weaker donor-acceptor interaction of the central TAPP unit with the nitrophenyl moieties. These electronic interactions cause a significant hypsochromic shift, along with a decrease in the fluorescence response (Table 15).[110]

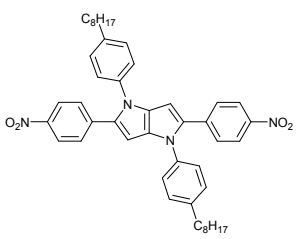

51

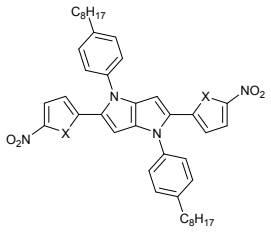

52, X = O
53, X = S

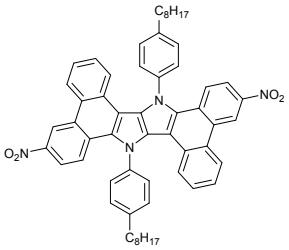

54

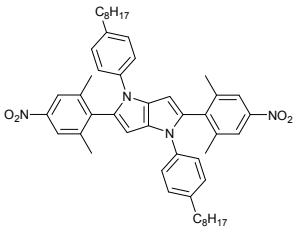

55

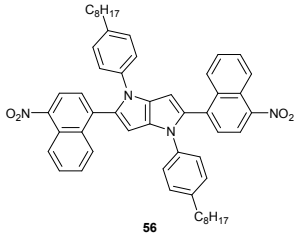

56

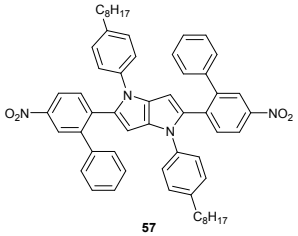

57

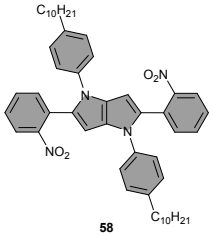

58

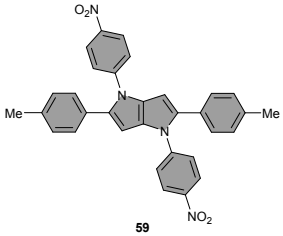

59

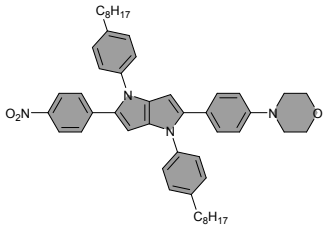

60

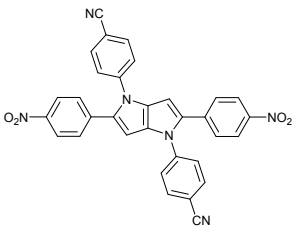

61

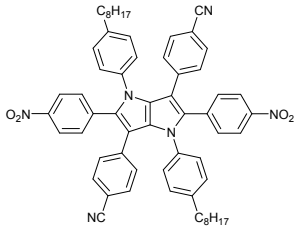

62

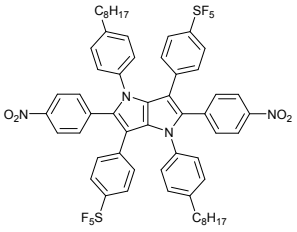

63

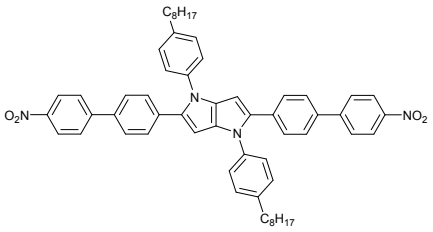

64

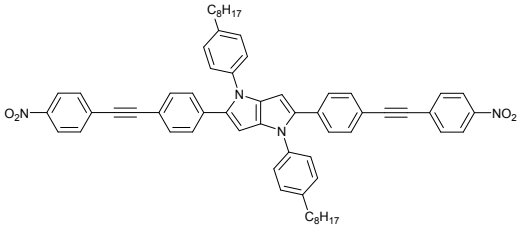

65

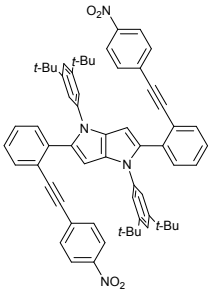

66

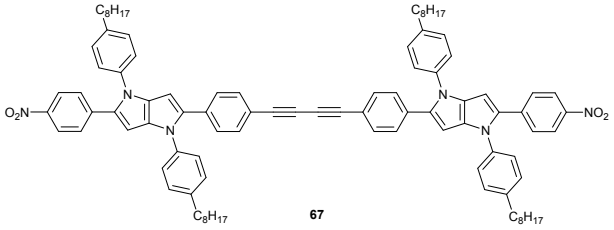

67

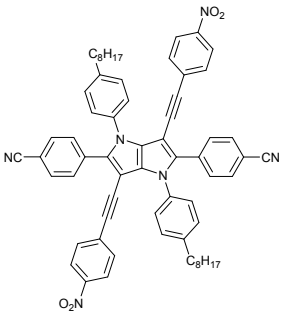

68

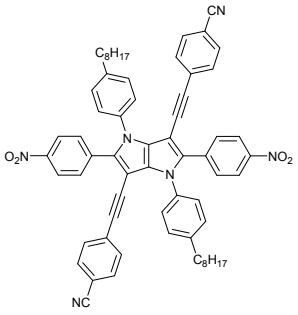

69

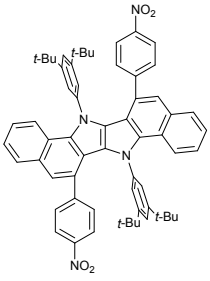

70

Fig. 22 Structures of tetraaryl-pyrrolopyrroles **51**-**70** possessing nitro group(s). Fluorescence of dyes colored in gray is below 0.001

Table 15 Photophysical properties of nitro-TAPPs **51**-**70**.

Compd	Solvent	λ_{abs} / nm	$\varepsilon \cdot 10^{-3}$ / $M^{-1} \cdot cm^{-1}$	λ_{em} / nm	$\Delta\bar{\nu}_s$ / cm^{-1}	Φ_f
51	C_6H_{12}	447, 469	48	496, 525	1200	0.96
	CCl_4	458	45	540	3316	0.93
	Toluene	465	42	552, 569	3400	0.70
	dioxane	464	44	590	4603	0.25
	THF	471	44	610	4800	0.03
	CH_2Cl_2	477	41	nd	nd	nd
	CH_3CN	467	40	nd	nd	nd
52	C_6H_{12}	479	47	525	1800	0.51
	Toluene	506	44	570	2200	0.15
	THF	508	49	595	2900	0.06
	CH_2Cl_2	530	nd	[c]	nd	[c]
	CH_3CN	512	nd	[c]	nd	[c]
53	C_6H_{12}	507	45	563	2000	0.14
	Toluene	532	47	605	2300	0.33
	THF	541	52	629	2600	0.20
	CH_2Cl_2	551	nd	[c]	nd	[c]
	CH_3CN	547	nd	[c]	nd	[c]
54	C_6H_{12}	473	52	484	500	0.80
	Toluene	480	50	518	1500	0.72
	THF	477	50	547	2700	0.54
	CH_2Cl_2	483	49	636	5000	0.06
	CH_3CN	479	13	661	5200	0.01
55	C_6H_{12}	406	nd	501	4700	0.22
	Toluene	414	10	564	6400	0.02
	THF	419	nd	[c]	nd	[c]
	CH_2Cl_2	425	nd	[c]	nd	[c]
	CH_3CN	413	nd	[c]	nd	[c]
56	C_6H_{12}	460	25	520	2500	0.54
	Toluene	464	22	576	4000	0.08
	THF	468	nd	[c]	nd	[c]
	CH_2Cl_2	476	nd	[c]	nd	[c]
	CH_3CN	461	nd	[c]	nd	[c]
60	C_6H_{12}	449	26	512	2700	0.59
	Toluene	461	27	566	4000	0.07
	THF	466	25	nd	nd	nd
	CH_2Cl_2	472	24	nd	nd	nd
	CH_3CN	462	24	nd	nd	nd
61	C_6H_{12} [b]	-	-	-	-	-
	Toluene	438	22	512	3300	0.97
	THF	447	nd	[c]	nd	[c]
	CH_2Cl_2	449	nd	[c]	nd	[c]
	CH_3CN	447	nd	[c]	nd	[c]
62	C_6H_{12}	432	33	476	2100	0.70
	Toluene	444	24	534	3800	0.25
	THF	449	27	600	5600	0.01
	CH_2Cl_2	460	27	nd	nd	0.00
	CH_3CN	450	25	nd	nd	nd
63	C_6H_{12}	433	31	476, 503	2100	0.32
	Toluene	443	27	535	3900	0.13
	THF	447	27	nd	nd	nd
	CH_2Cl_2	459	27	nd	nd	nd
	CH_3CN	448	24	nd	nd	nd
64	C_6H_{12}	439	50	513	3300	1.00
	CCl_4	446	42	577	5100	0.14
	toluene	444	41	610	6100	0.33
	dioxane	442	45	653	7300	0.082
	THF	446	43	~708	~8300	0.0023
	CH_2Cl_2	444	38	nd		
	CH_3CN	439	26	nd		
65	C_6H_{12}	449	59	515	3700	0.25
	Toluene	453	50	585	5000	0.03
	THF	450	54	nd	nd	0.00
	CH_2Cl_2	451	51	nd	nd	nd
	CH_3CN	440	47	nd	nd	nd
66	C_6H_{12}	452	7.4	578	4800	0.09
	toluene	410	12	496	4200	0.59
	CH_2Cl_2	441	5.6	-	-	-
67	C_6H_{12}	457	99	508	1500	0.28
	Toluene	466	84	568	3900	0.23
	THF	469	nd	[c]	nd	[c]
	CH_2Cl_2	472	nd	[c]	nd	[c]
68	toluene	379; 423	64; 39	540	5120	0.52[a]
					5120	0.33[b]
	$CHCl_3$	385; 430	50; 30	665	8220	<0.001
	CH_2Cl_2	384; 429	66; 43	-		<0.001
69	C_6H_{12}	358; 434; 461	50; 29; 25	481		0.75[a]
	toluene	363; 444	51; 30	561	4700	0.66[a]
	$CHCl_3$	368; 455	42; 24	665	7300	<0.001
	CH_2Cl_2	366; 453	51; 29	-		<0.001
70	C_6H_{12}	401	10	533	6200	0.22
	toluene	376	18	476	5600	0.25
	CH_2Cl_2	409	10	-	-	-

Considering the effects of the chromophore length, the analysis of the spectroscopic properties of a series of dinitro-TAPPs bearing additional linkers suggests that an increase in the distance between nitro groups and pyrrolo[3,2-*b*]pyrrole barely affects the absorption and fluorescence properties. Introduction of an additional benzene ring (**64**)[20] causes only a small hypsochromic shift without the loss of the absorption strength. Computational studies of this molecule reveal that the excited state experiences geometry changes to form a partially planar CT state, similar to its analog **51**. As biphenyl moieties allow for a larger geometry fluctuation, the Stokes' shifts tend to increase in comparison with analogue **51**, though the fluorescence responses of compounds **51** and **64** are quite similar.[20] In the case of the ethynyl linker (dyes **65**-**67**),[108, 110, 111] the spectroscopic behavior resembles that of **65**. Nevertheless, the fluorescence is partially quenched due to π–π and π*–π* energy mismatches at C(sp^1)–C(sp^2) connections and, hence, weakened conjugation between electron-donor and acceptor parts.[113] In contrast to TAPP **58**, the fluorescence of compound **66** with nitrophenyl-ethynyl units at the *ortho*-position is not completely quenched because the ethynyl linkers pull nitrophenyl moieties out of the central framework, making it possible to form a planar CT state.[108]

The extent of the conjugated chain has only a small effect on the position of the absorption and emission bands. The increased Stokes' shift in comparison with model pyrrolo[3,2-*b*]pyrrole **51** suggests significant geometry changes in the excited state following the photoexcitation. The fluorescence response in nonpolar media is relatively large because, for the TAPP chromophore, the ISC pathway is not preferred. Even a small increase in the solvent polarity, however, dramatically reduces the fluorescence efficiency as a CT state with the twisted geometry becomes considerably stabilized (Table 15).

The evaluation of the effect of structural variation on dinitro-pyrrolo[3,2-*b*]pyrroles suggests that the effective conjugation of nitro groups with the central scaffold tends to

increase the fluorescence response. The introduction of bulky moieties increases the dihedral angles between the chromophore core and nitrophenyl substituents, causing a decrease in the fluorescence efficiency. Likewise, an increase in the solvent polarity tends to stabilize CT states with the twisted geometry and hence quench fluorescence through IC.

A series of tetraethynylbenzene-based nitro-chromophores bearing both electron-donating and electron-withdrawing groups are reported to exhibit fluorescence (Figs. 23-25).[114, 115] Pulse radiolysis in benzene, generating simultaneously the singly oxidized and singly reduced forms of these conjugates, provides mechanistic insights about their emission.[114] Bimolecular charge recombination between the radical cations and the radical anions leads to the formation of the singlet excited states of these dyes, which undergo radiative deactivation.[114] The distributions of the frontier orbitals of these tetraethynylbenzene conjugates are consistent with the CT character of the singlet excited state, showing noticeable HOMO-LUMO overlap only over the central benzene unit.[115] Therefore, the medium polarity and the configuration of their electron donating and accepting moieties strongly affects their fluorescence. The fluorescence response was quite substantial for nonpolar solvents, such as toluene, and was quenched upon an increase in medium polarity (Tables 16-17).

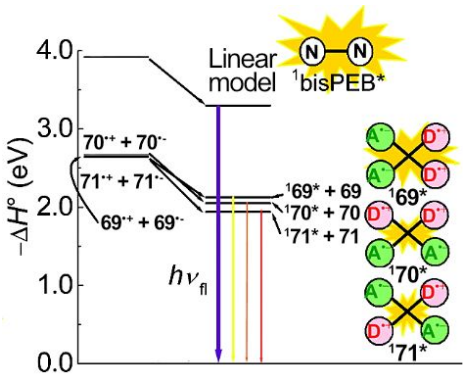

Fig. 23. Energy level diagram for radiolysis induced chemiluminescence of dyes **69**-**71** . Adapted with permission from Ref. [114] Copyright 2007 American Chemical Society.

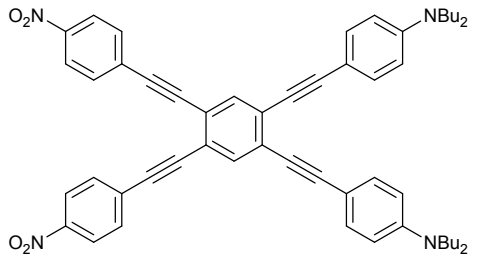

71

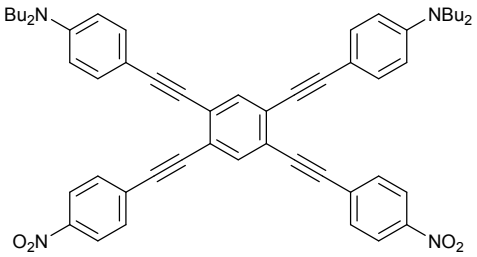

72

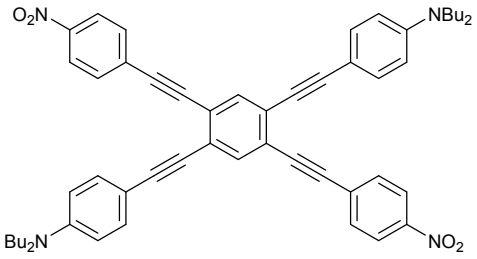

73

Fig. 24. Structure of cross-shaped chromophores **71-73.**

Table 16 Steady-state spectral properties of compounds **71**-**73** in Ar-saturated benzene

compd	λ_{em} / nm	λ_{em} / nm	$\Delta\bar{\nu}_s$ / cm^{-1}	E_{SI} [a] / eV	Φ_f	τ_f / ns
71	326, 417	594	7100	2.09	0.36 ±0.01	3.6
72	325, 421	610	7400	2.03	(5.1 ±0.2) · 10^{-3}	2.0
73	313, 383, 446	643	6900	1.93	(4.8 ±0.1) · 10^{-4}	0.067

[a] Estimated from the peak wavelength of the fluorescence spectra (10^{-5} M).

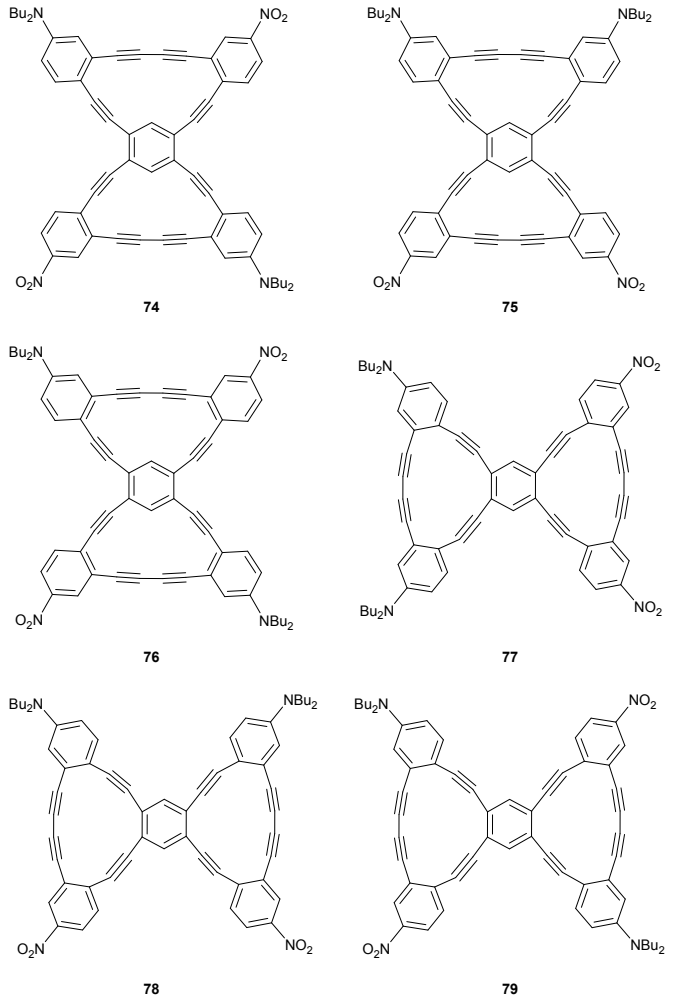

Fig. 25 Structures of nitro-aromatics **74-79.**

Table 17 The photophysical data for dyes **74**-**78**

compd	Solvent	λ_{abs} / nm ($\varepsilon \cdot 10^{-3}$ / $M^{-1}cm^{-1}$)	net dipole (D)a	λ_{em} / nm	$\Delta\bar{\nu}_s$ / cm^{-1}	Φ_f
74	Toluene	319 (58); 456 (30)	15.06	565	4200	0.11
75	Toluene	318 (99); 491 (57)	18.34	560	2500	0.17
75·HCl	CH_2Cl_2	308 (114); 430 (46)	b	517	3900	0.31
76	Toluene	330 (91); 415 (41); 473 (29)	0.00	580	3900	0.06
77	Toluene	326 (71); 453 (34)	15.26	560	4200	0.10
78	Toluene	325 (69); 466 (41)	18.33	560	3600	0.09

In the case of the pyrrolo[3,2-*b*]pyrrole core discussed above, the formation of an excited state with a CT character fully controls the photophysics of the centrosymmetric dyes. Intuitively, the driving force for the electron density shift upon excitation (hence the formation of a dark, CT-type state) may be controlled mostly through the electron-donating ability of the central scaffold of the molecule, which would ideally lead to fluorescence enhancement.

Diketopyrrolopyrroles (DPPs) are a class of organic colorants known for their superb optoelectronic properties and persistence towards ambient conditions.[116] The introduction of various functionalities into positions 3 and 6 strongly adjusts their optical behavior, while changing the substitution character at positions 2 and 5 (at nitrogen atoms) negligibly affects this behavior.[117, 118] Recently, we described two DPP-based dyes possessing nitro group(s) (Fig. 26) that feature unusually strong emission, with maxima reaching 750 nm and $\Phi_f \approx$ 0.39-0.80 in toluene (Table 18).[119] The high emission intensity clearly benefits from the lack of electronic coupling between the DPP core and nitropyridine-based groups placed on the nitrogen atoms, as confirmed by theoretical calculations (Fig. 27). On the basis of TAS, we proposed a reliable kinetic model (Fig. 28) for the optical behavior of DPPs. In toluene, the initial excitation to the (S_1) state is followed by population of the long-lived $(S_1)_{SOL}$ state (related to solvent reorganization) and the short-lived $(S_1)_{STR}$ state (related to structural relaxation) (Table 17). The $(S_1) \rightarrow (S_1)_{SOL}$ transition corresponds to the reduction of the solvation

energy of the excited state, while the latter one ($(S_1) \rightarrow (S_1)_{STR}$) results from reorganization of the potential energy surface and is likely to possess a sizeable contribution from the redistribution of charge density. Those states are close in energy and are populated simultaneously. In benzonitrile, the initial photoexcitation pathway remains the same, that is, $(S_1)_{SOL}$ is populated through the (S_1) state. Here, the polar environment significantly stabilizes the $(S_1)_{STR}$ state (the energy of this state decreases), making it long-lived, while, $(S_1)_{SOL}$ decays on a picosecond timescale. In both solvents, the photophysical scenario ends up with decay to the excited triplet state (T_1) through ISC followed by recovery of S_0. To summarize, efficient population of the $(S_1)_{STR}$ state with a sizeable charge-transfer contribution, along with ISC, are the main events responsible for the low emission of **80** and **81** in benzonitrile.

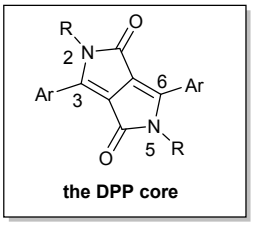

the DPP core

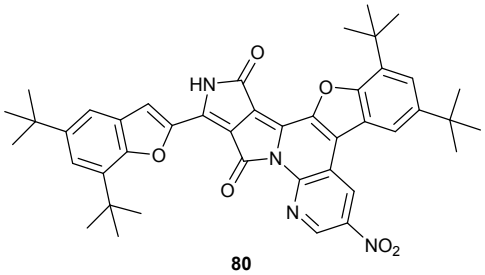

80

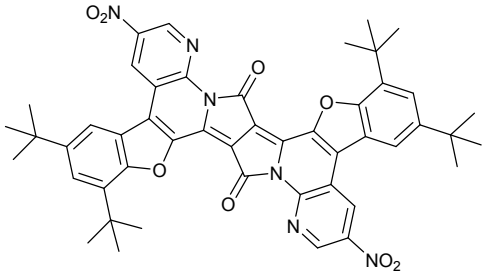

81

Fig. 26 Structures of dyes **80** and **81** based on the DPP core.

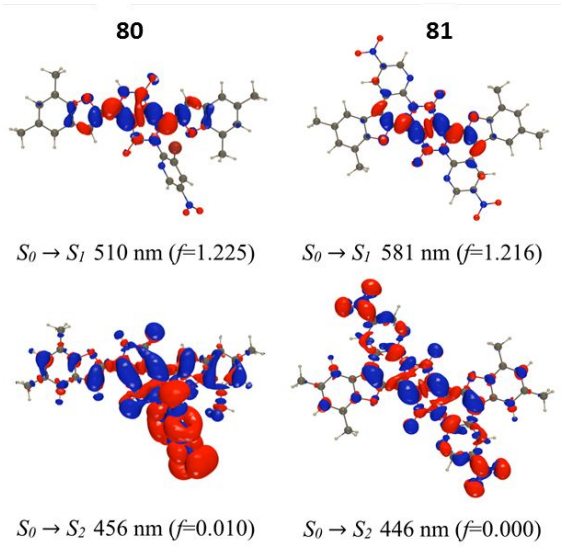

Fig. 27 M06-2X density difference plots for the two lowest lying FC excited states of dyes **80** and **81** The relatively large size of the DPP core and its electron-deficient character (compared with the pyrrolo[3,2-*b*]pyrrole core) result in local character of the $S_0 \rightarrow S_1$ (HOMO → LUMO) transition, which occurs exclusively within the DPP core.

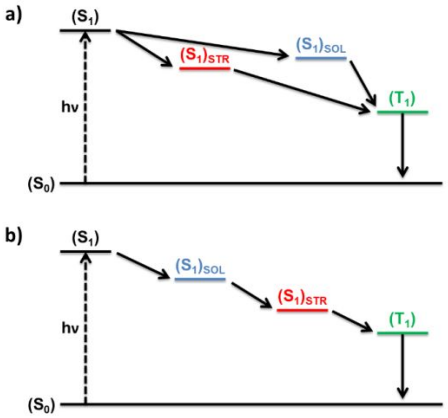

Fig. 28 Kinetic models in the GloTarAn target analysis for fitting the transient absorption data of **80** and **81** in a) toluene and b) benzonitrile

Table 18 Optical data for compounds **80** and **81**

cmpd	solvent	λ_{abs} / nm	λ_{em} / nm	$\Delta\bar{\nu}_s$ / cm^{-1}	Φ_f	τ_f / ns	$k_r \cdot 10^{-8}$ / s^{-1} [a]	$k_{nr} \cdot 10^{-8}$ / s^{-1} [b]	$\tau(S_1)$ / ps	$\tau(S_1)_{STR}$	$\tau(S_1)_{SOL}$ / ns	$\tau(T_1)$ / µs
80	PhMe	609; 556	615; 676		0.39	4.1	0.95	1.5	1.38	269.38 ps	2.86	21.89
	PhCN	-	-	-	0.006	<0.2	-	-	8.60	22.03 ns	24.30 ps	117.56
81	PhMe	657; 595	663; 735		0.88	3.7	2.4	0.32	8.60	228.41 ps	3.93	69.94
	PhCN	-	-	-	0.032	<0.2	-	-	3.17	13.82 ns	143.00 ps	4.16

[a] $k_r = \Phi_f / \tau_f$; [b] $k_{nr} = (1 - \Phi_f) / \tau_f$

Similarly, the local character of the $S_0 \rightarrow S_1$ transition mostly dominates the optical behavior of nitroaryl-substituted dipyrrolonaphthyridinediones (DPNDs) **84**-**94** (Fig. 29)[11]. In line with our previous study,[120] the DPND core (dye **82**) as a whole behaves as a weak electron acceptor, eventually preventing a significant shift of the electron density toward the nitro group and giving rise to strongly fluorescent nitroaromatics. Conjugates of the acceptor-'acceptor'-acceptor (**89**-**94**) or acceptor-'acceptor' type (**84**-**88**) fluoresce mainly in non-polar solvents and also in relatively dipolar dichloromethane with quantum yields up to 0.76 (among dipolar molecules) and 0.95 (among quadrupolar molecules), while in polar CH_3CN almost

all derivatives are weakly fluorescent. Theoretical calculations unveil an unexpected photochemical reactivity of **89**-**94** in the excited state. Namely, the lowest lying S_1 state, which is fluorescent and has a $^1\pi\pi^*$ character, may adiabatically transit to ^{1}CT or $^1n\pi^*$ state involving, respectively, dihedral twisting of the *ortho/peri*-nitro or *para*/*meta*-nitroaryls attached to the DPND chromophore core. Thus, these non-fluorescent ^{1}CT and $^1n\pi^*$ structures become the lowest lying singlet excited states that efficiently undergo non-radiative deactivation through a conical intersection (CI) with the S_0 state. Computational analysis reveal that the twisting around the C_{aryl}-N bond in the ^{1}CT and $^1n\pi^*$ states, leading to the CI, results a transitory formation of a covalent C-O bond. The increase in medium polarity enhances the driving force for forming this new C-O bond. This bond breaks upon relaxation from the CI to the optimal ground-state geometry, which is consistent with *aborted photochemistry* (Fig. 30).[11]

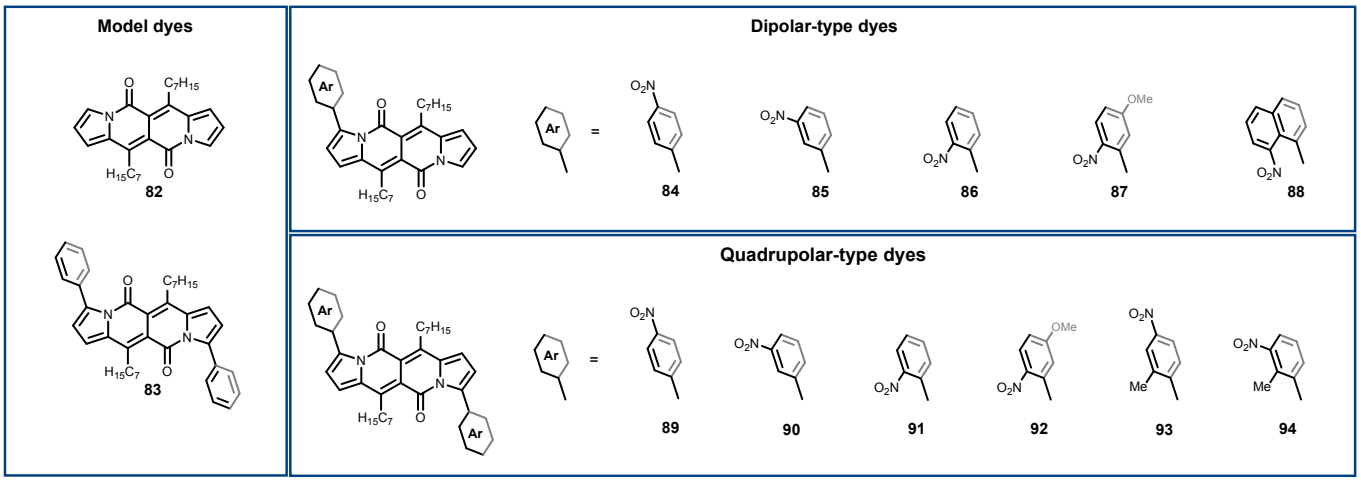

Fig. 29 The structures of bis(nitro)DPNDs **84**-**94** and parent DPNDs **82** and **83**.

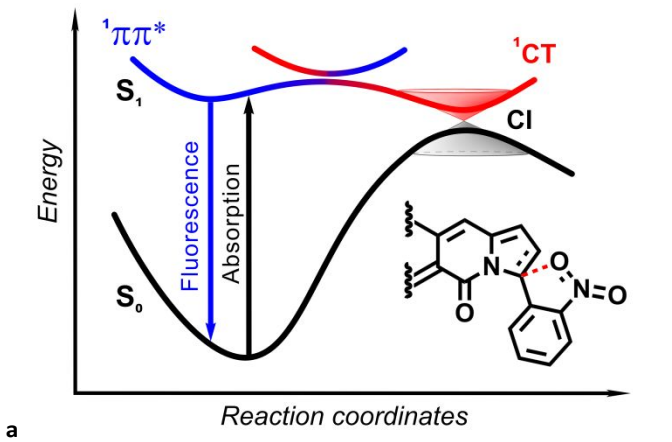

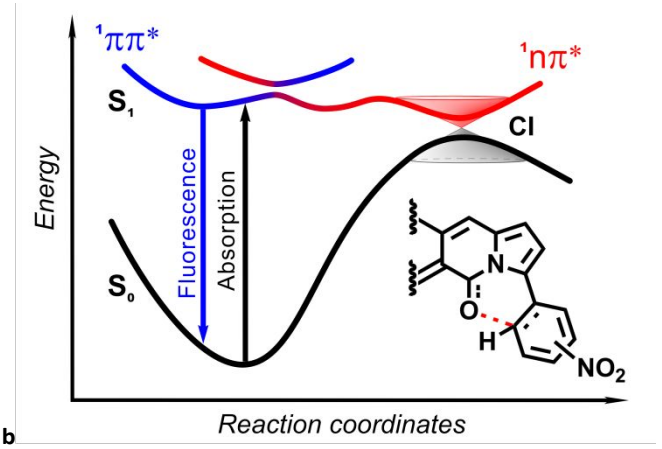

Fig. 30 Schematic diagrams showing the general scenarios of temporal evolution of the photoexcited nitroaryl substituted DPNDs. (a) Excited-state dynamics of *ortho*-nitrophenyl (and *peri*-nitronaphthyl) derivatives of DNPD. Optical electronic excitation produces locally excited (LE) state with a $^1\pi\pi^*$ character that adiabatically transitions to a CT twisted state along the S_1 potential-energy trajectory. The photoexcited dyes either deactivate radiatively from $^1\pi\pi^*$ to S_0 or non-radiatively through $^1\pi\pi^*\rightarrow{}^1CT\rightarrow S_0$ transitions. (b) evolution of photoexcited *meta*- and *para*-nitrophenyl substituted DPNDs. Upon photoexcitation, the initially formed fluorescent $^1\pi\pi^*$ state adiabatically transitions to a twisted non-fluorescent $^1n\pi^*$ state along the S_1 potential-energy trajectory. The $^1n\pi^*$ S_1 state forms a CI with the ground state, which accomodtes non-radiative deactivation, i.e., $^1\pi\pi^*\rightarrow{}^1n\pi^*\rightarrow S_0$. (CI = conical intersection)

This work undoubtedly points to a new paradigm for the fluorescence quenching mechanisms in nitroaromatics. This type of *aborted photochemistry* pathway for non-radiative

deactivation was predicted theoretically in the 1990s,[121, 122] but only recently demonstrated experimentally.[123, 124]

In addition to the deactivation along the singlet manifold, TAS measurements reveal that non-radiative depopulation of the S_1 state through ISC is also possible for DPNDs containing *ortho/peri*-nitroaryls at the peripheries. In contrast, the decays of the photoexcited *meta/para*-nitrophenyl DPNDs do not lead to detectable formation of triplets, even though their S_1 states undergo dihedral twist transitioning to $^1n\pi^*$ configuration. These findings have an important implication for the non-radiative deactivation of chromophores modified with nitroaryl substituents. As numerous examples demonstrate, dihedral twisting of biaryl linkers leads to the formation of CI between S_1 and S_0 states that accommodates efficient non-radiative deactivation without changing multiplicity. Placing nitro groups at *ortho* or *peri* position in relevance to the biaryl σ-bond, indeed, enhances this CI-mediated deactivation because of the twisted geometries that the steric hindrance induces. In addition, the *ortho* and *peri* locations of the nitro groups place their oxygens spatially close to the π-orbitals of the chromophore cores. This proximity provides coupling for through-space electron transfer (ET), which is important not only for the formation of the CT states and for their deactivation via back ET, but also for transferring the hole between the n orbital on the -NO_2 oxygen and the π orbital on the chromophore core needed for ISC. The latter is consistent with our findings that the inherently twisted geometries of chromophores with *ortho*- and *peri*-nitroaryl substituents exhibit enhanced SOC and increased rates of ISC.[11, 20]

Photoinduced electron transfer strategy for controlling fluorescence

As we discuss and illustrate with numerous examples in the previous sections, the importance of intramolecular charge transfer for the photophysics of nitroaromatics cannot be overstated. Ground-state CT leads to the polarization inherent for the S_0 structures of nitroaromatics. It is the excited-state CT processes, however, that alter this polarization and affect the photophysics. Photoinduced charge transfer (PCT) describes light initiated displacement of charges, such as photoinduced electron transfer (PET), photoinduced hole transfer (PHT) and photoinduced proton transfer (PPT).[18] While PET and PCT are often used interchangeably, we ought to emphasize that PET is a type of PCT, i.e., not all PCT processes are PET. Neverthless, because optical excitation of nitroaromatics usually involves NTOs localized mostly on their electron-rich chromophore cores, i.e., photoexciting the electron donors, PET is what governs their excited-state dynamics.

PCT and, in particular, PET[125-129] are non-radiative processes that can effectively contribute to a decrease in the fluorescence lifetimes and fluorescence quantum yields of organic molecules, and/or induce pronounced bathochrmic shifts. PCT leading to dark CT states, i.e., states with well separated charges, quenches fluorescence. Conversely, when the electron and the hole NTOs of a CT state overlap, PCT leads to bathochromically shifted CT→S_0 fluorescence that is susceptible to changes in solvent plarity. The formation of fluorescent CT states is not limited to intramolecular PCT. Exciplex formation and emission illustrate how intermolecular PCT can lead to fluorescent bimolecular CT states.

When a molecule contains an electron donor (D) and an electron acceptor (A) that are weakly coupled with each other, an intramolecular PCT may occur after the photoexcitation and the relaxation of the Franck-Condon, FC, to a locally excited, LE, state.[130, 131] When the donor-acceptor electronic coupling is strong, a direct photoexcitation to the CT state can become possible. That is, in addition to the absorption leading to the LE state, which is not truly susceptible to solvent polarity, a bathochromically shifted CT band, originating from the S_0→CT transition and manifesting pronounced solvatochromism, appears in the spectra.[132, 133]

The Rehm-Weller equation provides a means for characterizing the thermodynamics of PCT processes from experimentally obtainable characteristics of the donor and the acceptor. For non-charged donors and acceptors (eq. 5).[134, 135] The estimated change that PCT induces in the Gibbs free energy of the optically excited systems ($\Delta G_{PCT}^{(0)}$) comprising non-charged donor and acceptor amounts to:[136, 137]

$$\Delta G_{\mathrm{PCT}}^{(0)}(\varepsilon, n^2) = F\left(E_{\mathrm{D}^{\bullet+}|\mathrm{D}}^{(0)}(\varepsilon_{\mathrm{D}}) - E_{\mathrm{A}|\mathrm{A}^{\bullet-}}^{(0)}(\varepsilon_{\mathrm{A}})\right) - \Delta\mathcal{E}_{0,0}(\varepsilon, n^2) + \Delta G_S(\varepsilon, \varepsilon_{\mathrm{D}}, \varepsilon_{\mathrm{A}}) + W(\varepsilon) \quad (5)$$

where $E_{\mathrm{A}|\mathrm{A}^{\bullet-}}^{(0)}(\varepsilon_{\mathrm{A}})$ and $E_{\mathrm{D}^{\bullet+}|\mathrm{D}}^{(0)}(\varepsilon_{\mathrm{D}})$ are the single-electron reduction potentials of the acceptor and the oxidized donor obtained for solution media with static dielectric constants ε_A and ε_D, respectively; $\Delta\mathcal{E}_{0,0}(\varepsilon, n^2)$ is the zero-to-zero energy for the optical excitation to the S_1 LE state obtained for medium with a dielectric constant ε and a refractive index n; $\Delta G_S(\varepsilon, \varepsilon_D, \varepsilon_A)$ is the Born solvation term accounting for the interaction between the donor and the acceptor with the surrounding media and correcting the reduction potentials from values for ε_D and ε_A to values for ε;[136] : $W(\varepsilon)$ is the Coulombic work term accounting for the electrostatic interactions between the oxidized donor and the reduced acceotor, which strongly depends on the distance between them; and F is the Faraday constant relating the potetnials to the energy values.

The thermodynamic driving force of PCT, which is quantified by the negative values of $\Delta G_{PCT}^{(0)}$, illustrates how low under the LE state is the energy level of the CT states. Equation 5 shows that all the terms defining the PCT driving force depend on the polarity of the solvating media,[137] as implemented by the Born solvation model[138] for the reduction potentials and ΔG_S, by the Coulombic model[139-141] for W, and by the Onsager solvation model[142] (accounting for the solvatochromism of the LE state) for $\Delta\mathcal{E}_{0,0}$. Permanent electric dipoles of moieties attached to donor-acceptor conjugates further modulate $\Delta G_{PCT}^{(0)}$.[143]

For molecules in which the nitro-containing moiety plays a role of an electron acceptor, the principal chromophore core is usually electron-rich enough to act as an electron donor. Commonly, the HOMO-LUMO energy gap of the donor is smaller than that of the nito-containing acceptor and the LUMO of the acceptor is below the LUMO of the donor (Fig.

31a). This configuration readily mediates photoinduced electron transfer. Specifically, photoexcitation of the donor moves an electron to its LUMO, which can either recombine with the hole and radiatively relax to the ground state, or undergo PET by moving to the LUMO of the acceptor (Fig. 31a). Optical excitation of the acceptor at shorter wavelengths can induce hole transfer to the donor, which involves transduction of an electron from the HOMO of the donor to the hole NTO of the photoecited acceptor. Introducing the $\Delta\mathcal{E}_{0,0}$ of the donor in eq. 5 yields the driving force of PET, i.e., $-\Delta G_{PCT}^{(0)}$, and the $\Delta\mathcal{E}_{0,0}$ of the acceptor in eq. 5 produces the driving force of the photoinduced hole transfer, i.e., $-\Delta G_{PHT}^{(0)}$.[18] PHT, however, is usually slower than energy transfer from the electron acceptor to the donor, setting the stage for PET. For dyes containing nitrophenyl substituents, therefore, PET governs the excited-state dynamics (Fig. 31a).[88] When the formed CT state has biradical nature with well separated charges, radiative emission to the ground state is forbidden. Therefore, the PET process constitutes a competitive nonradiative de-excitation channel where the charge recombination leads to the ground state or to low-lying triplet states.[144]

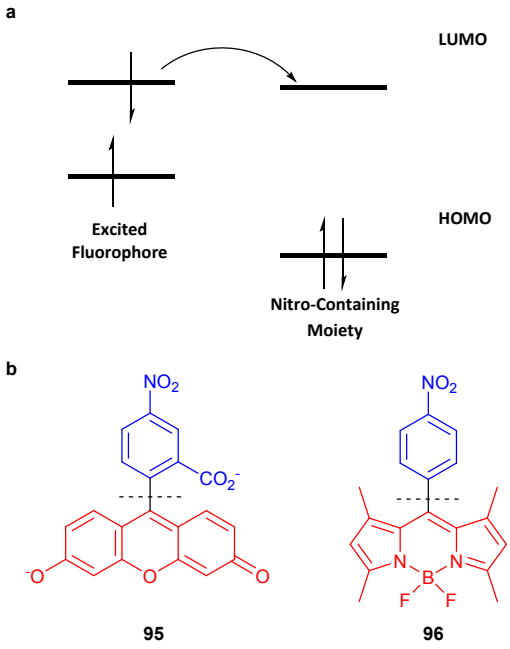

Fig. 31 a. The mechanism of donor-excited photoinduced electron transfer (d-PET). b. Examples of chromophores in which electron-accepting and electron-donating parts are electronically disconnected

The structure of typical dyes belonging to either the fluorescein[145] or BODIPY families can be divided into a chromophore unit (the xanthene or the BODIPY skeleton) and a benzene moiety (Fig. 31b). These two aromatic components are practically orthogonal to each other, which makes it safe to assume that the electronic coupling between them is immensely weak. Placing a nitro group on the benzene moiety efficiently lowers its LUMO level to assume a donor-acceptor configuration (Fig. 31a), which should quench the fluorescence *via* a PET mechanism. Based on this train of thought, Nagano *et al*.[146] hypothesized that, for a set of similar structures (in terms of a donor-acceptor distance and the electronic coupling between them), it may be possible to adjust the fluorescence properties essentially by altering the values of $E^{(0)}_{A|A^{\bullet-}}$ and $E^{(0)}_{D^{\bullet+}|D}$ (eq. 5) of the fluorophore and the nitroaryl moiety, respectively. For BODIPY dyes **97**-**100** bearing a 3-nitroaryl moiety (Fig. 32), the authors altered the reduction potentials by distinct structural modifications of both parts, which varied the PET driving force. As the PET become more endergonic, the fluorescence quantum yield rose sharply, reaching 0.53 (for molecule **99** in methanol) or 0.69 (for molecule **100** in acetonitrile).

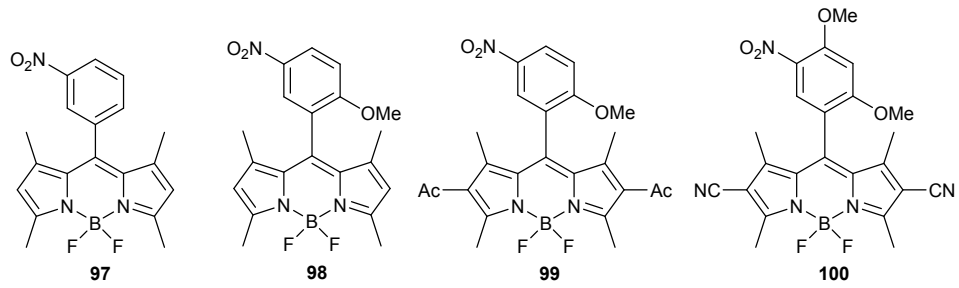

	97	**98**	**99**	**100**
Φ_f	0.004	0.023	0.529	0.687
Relative ΔG_{PET} / eV	0	+0.15	+0.42	+0.79

Fig. 32 Structures of 5-(nitrophenyl)BODIPYs **97**-**100**.

Otani and Saito proposed that the same type of quenching mechanism applies to a molecule bearing the pyrrolo[1,2-*a*][1,8]naphthylidine chromophore (**101**) and a 3-nitroaryl moiety[147] (Fig. 33). This biaryl link between the donor and the acceptor, however, does not guarantee an orthogonal arrangement. Compound **101** is virtually non-luminescent in dichloromethane. According to the authors, protonation at position N-14 increases the reduction potential of the oxidized donor, $E^{(0)}_{D^{\bullet+}|D}$ (eq. 5). That is, this protonation lowers the LUMO level of the pyrrolo[1,2-*a*][1,8]naphthylidine chromophore below the LUMO of the nitrophenyl moiety, which inhibits the PET process and allows fluorescence enhancement (Φ_f = 0.34 for **101**+H$^+$). DFT studies confirm almost complete spatial separation of the frontier orbitals within **101**, as the HOMO level is localized over the chromophore, while the LUMO lies exclusively within the 3-nitroaryl moiety. After the protonation event, both, the HOMO and the LUMO are localized predominantly within the principal chromophore core.

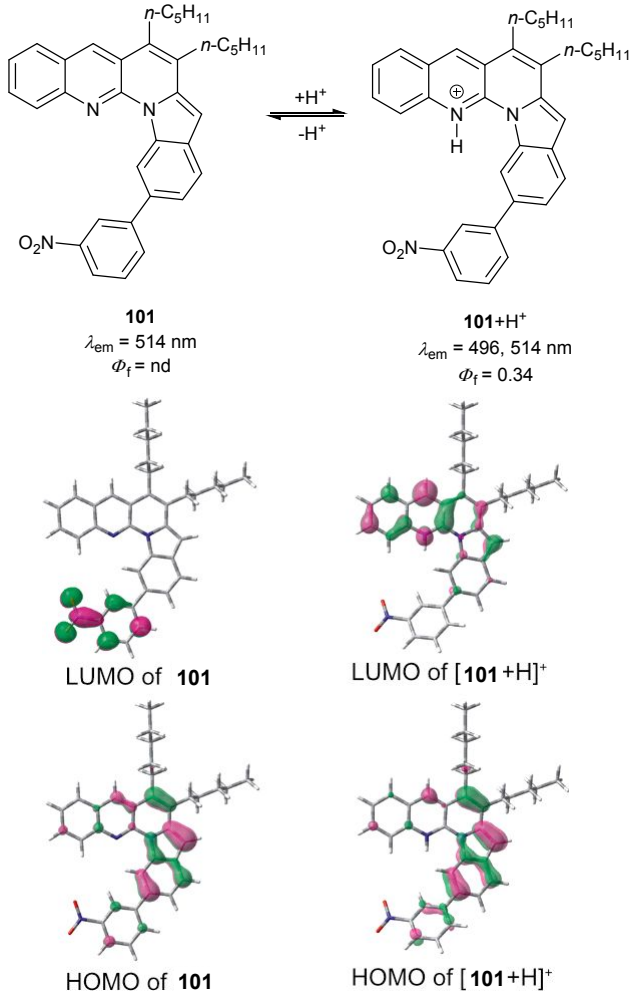

Fig. 33 Chemical structures as well as HOMOs and LUMOs of **101** and its 14-N protonated cation [**101**+H]$^+$. nd – not determined. Adapted with permission from Ref. [147] Copyright 2014 American Chemical Society.

How to make nitroaromatics fluoresce?

Care must be taken in attempts to optimize the fluorescence properties of nitroaromatics to avoid the emergence of undesirable alternative pathways for non-radiative deactivation (Fig. 34). Perhaps before attempting to answer the key question, it is important to recommend some general approaches for designing nitroaromatics that exhibit strong fluorescence based on what is discussed in this review. It is clear that solvent polarity strongly affects the fate of these molecules in their excited state. Inherently, nitroaromatics possess dipolar or quadrupolar architecture. As discussed, enhancing the CT character of the excited states decreases the SOC because of the decreased overlap between n orbital on the $-NO_2$ electron acceptor and the π orbital on the chromophore core that acts as an electron donor, (An electron transfer between an n and a π orbital has to accompany the spin flip in order to conserve the momentum during ISC.) Furthermore, CT-induced symmetry breaking in the excited state converts the quadrupolar to dipolar structures. Therefore, understanding the interplay between ISC, CT and radiative $S_1 \rightarrow S_0$ deactivation is paramount for making nitroaromatics fluoresce.

The picture can be somewhat "simplified" for non-polar media where the CT excited-states are not sufficiently stabilized and two possible scenarios are at play: weak SOC resulting in strong fluorescence, and strong SOC leading to weak fluorescence. That is, the focus is on ISC as the principal pathway of non-radiative deactivation that competes with the fluorescence decay.

An increase in solvent polarity, however, brings the CT states into the interplay of the excited-state dynamics and warrants increased caution when designing fluorescent nitroaromatics. Separating the n orbitals on the nitro group from the π orbitals on the chromophore core is essential for decreasing SOC, but such configurations also separate the NTOs for radiative deactivation of the CT state. That is, polarized CT states can quench the fluorescence not by enhancing the non-radiative rates but by suppressing the radiative ones. In addition, dihedral degrees of freedom between the electron accepting and donating moieties provides routes for their structures to evolve into TICT states. In addition to separating the NTOs and lowering the rates of radiative deactivation, such twisted states are prone to formation of conical intersection with the ground state, opening alternative routes of efficient non-radiative decays. In addition to a decrease in the CT character of the excited state (by adjusting not only the solvent polarity, but also the reduction potentials of the electron donating and accepting moieties), an increase in medium viscosity can also suppress the formation of TICT structures.

Placing the nitro groups on *ortho* or *peri* positions of nitroaryl substituents even further increases the complexity of the excited-state dynamics. Indeed, the steric hindrance introduced by the nitro groups in such conjugates enhances their propensity for formation of TICT states with pronounced orthogonality leading to negligibly small rates of radiative deactivation and immensely efficient internal conversion to the S_0 state via back CT. Placing the nitro groups right next to the electron rich chromophore core in such orthogonal structures, however: (1) decreases the donor-acceptor distance, which further stabilizes the CT state and enhances its susceptibility to solvent polarity as the Coulombic term, $W(\varepsilon)$, in eq. 5 illustrates; and (2) offers through-space donor-acceptor coupling, which not only increases the rates of PCT and back CT, but also enhances the SOC. The reason why CT states suppress ISC is because of the separation between the n and upper lying π orbitals, i.e., the π orbitals are localized on the electron donor and the n orbitals are well localized on the oxygens of the nitro group. Placing the nitro group spatially right next to the electron-rich core brings these localized n and π orbital close together, enhancing their overlap and the SOC. Therefore, while *ortho* and *peri* nitroaryl dyes exhibit not only slow radiative-decay rates and fast internal conversion (as expected for such twisted structures), but also unusually fast ISC (Fig. 34d).[11, 20]

Even when the CT character of the excited states is well balanced to suppress ISC without quenching the fluorescence by forming dark TICT states, the close energy levels of low laying $^1\pi\pi^*$ and $^1n\pi^*$ excited states can open alternative pathways of deactivation that are enhances by solvent polarity (Fig. 30b).

Assuming that one can freely manipulate the chromophores through structural modifications, based on the presented discussion, the following principles for achieving reasonably intense fluorescence in the desired range of solvents can be enunciated:

1) Lower the energy level of the S_1 state below that of T_2 and the other upper triplet states (Fig. 34a,b).

2) Make sure that the energy levels of the lowest $^1\pi\pi^*$ and $^1n\pi^*$
excited states are well separated. In addition to preventing $^1\pi\pi^* \rightarrow {}^1n\pi^*$ deactivation pathways (Fig. 30b), it will make it more likely for the $^3n\pi^*$ ($^3\pi\pi^*$) triplet states to be above the $^1\pi\pi^*$ ($^1n\pi^*$) S_1 state.

3) Suppress the electronic coupling with the nitro group, e.g., place $-NO_2$ at a node of the frontier orbitals (the nitro group will still make the compound electron deficient, but only inductively).

4) Most importantly, induce charge-transfer character to suppress ISC, but not too much, in order to prevent the formation of dark TICT states (Fig. 34c,d). The twisted excited states not only form conical intersections with the ground state that accommodate efficient non-radiative deactivation, but also enhance the rates of ISC when the nitro group is at the *ortho* or *peri* position on the aryl substituent (Fig. 34 d).[11, 20]

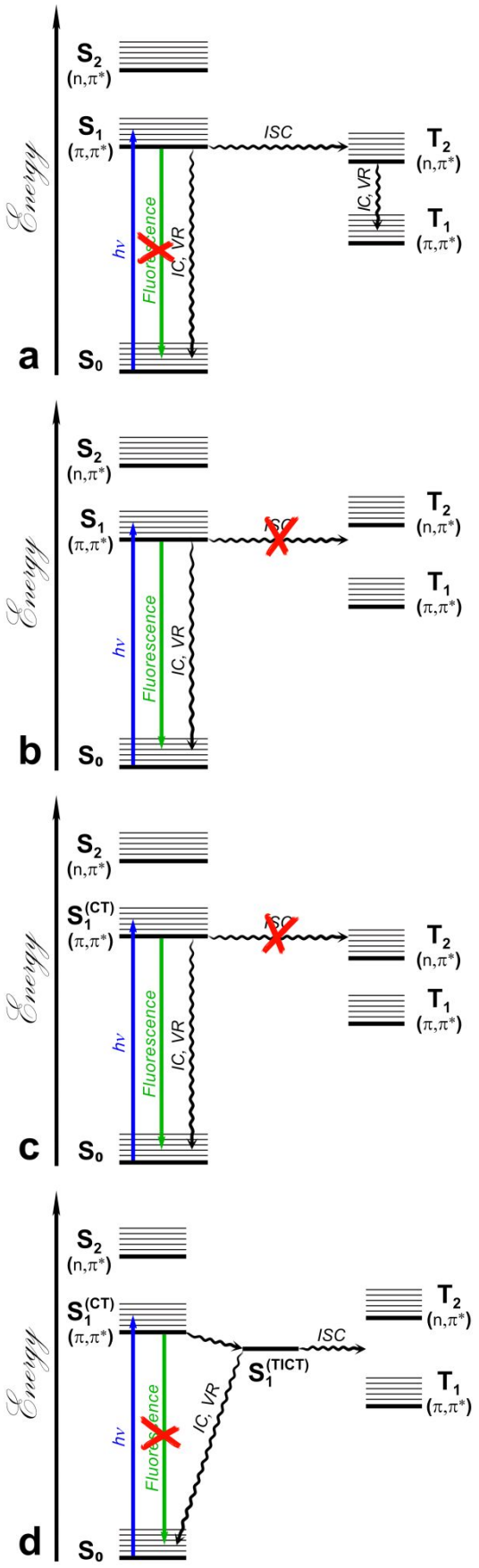

Fig. 34 Jablonski diagrams illustrating possible deactivation pathways of photoexcited nitroaromatic chromophores. (ISC = intersystem crossing, IC = internal conversion, and VR = vibrational relaxation)

Summary and outlook

Forty years ago, it would have been impossible to imagine that it would only take a few decades for our understanding of the fluorescence of nitroaromatic compounds to expand into an independent field of study. This progress was possible due to the simultaneous rise in synthetic methodology, computational resources and time-resolved spectroscopy. Intense work after 2000 led to crystallization of a few distinct strategies, leading to fluorescence enhancement in nitroaromatics. One can venture to hypothesize that the field is now mature enough to move to the next level, i.e., to design new, strongly fluorescent nitroaromatics *in silico*. Such a scenario is most probably just around the corner and it indeed may come to fruition in the near future. Adding the -NO_2 functional group to the existing toolbox currently used by scientists working in the field of organic fluorophores will, no doubt, bring rapid advancements as the possibilities for molecular design increase. Many key questions still remain, however, and perhaps new mechanisms of excited-state deactivation are still to be discovered. Nevertheless, analysis of research performed since the beginning of the 21st century suggests that the variety and novelty of future fluorescent nitroaromatic chromophores will be limited only by our imagination.

Author Contributions

All authors equally contributed to writing the manuscript.

Conflicts of interest

There are no conflicts to declare.

Acknowledgements

The work was financially supported by the Polish National Science Centre, Poland (PRELUDIUM 2016/23/N/ST5/00054, HARMONIA 2016/22/M/ST5/00431), the Foundation for Polish Science (TEAM POIR.04.04.00-00-3CF4/16-00 and START scholarship no. 076.2020 to B.S.), the USA National Science Foundation (grant number CHE 1800602), the American Chemical Society Petroleum Research Fund (grant number 60651-ND4), and the USA National Institutes of Health, National Eye Institute (grant R01 EY027440). F.H.Q thanks the CNPq, Brazil, for a research productivity fellowship.

Notes and references

1. T. M. Wilson, M. J. Tauber and M. R. Wasielewski, *J. Am. Chem. Soc.*, 2009, **131**, 8952-8957.
2. M. Stolar and T. Baumgartner, *Phys. Chem. Chem. Phys.*, 2013, **15**, 9007-9024.
3. Q. Yue, W. Liu and X. Zhu, *J. Am. Chem. Soc.*, 2020, **142**, 11613-11628.
4. A. Ashcraft, K. Liu, A. Mukhopadhyay, V. Paulino, C. Liu, B. Bernard, D. Husainy, T. Phan and J. H. Olivier, *Angew. Chem. Int. Ed.*, 2020, **59**, 7487-7493.
5. J. Anthony, A. Facchetti, M. Heeney, S. Marder and X. Zhan, *Adv. Mater.*, 2010, **22**, 3876-3892.
6. C. Hansch, A. Leo and R. W. Taft, *Chem. Rev.*, 1991, **91**, 165-195.
7. E. M. Espinoza, B. Xia, N. Darabedian, J. M. Larsen, V. Nuñez, D. Bao, J. T. Mac, F. Botero, M. Wurch, F. Zhou and V. I. Vullev, *Eur. J. Org. Chem.*, 2016, **2016**, 343-356.
8. K. Rybicka-Jasińska, E. M. Espinoza, J. A. Clark, J. B. Derr, G. Carlos, M. Morales, M. K. Billones, O. O'Mari, H. Ågren, G. V. Baryshnikov and V. I. Vullev, *J. Phys. Chem. Lett.*, 2021, **12**, 10295-10303.
9. Y. Wu, D. Kim and T. S. Teets, *Synlett*, 2022, DOI: 10.1055/a-1390-9065.
10. M. C. Chen, D. G. Chen and P. T. Chou, *ChemPlusChem*, 2021, **86**, 11-27.
11. B. Sadowski, M. Kaliszewska, Y. M. Poronik, M. Czichy, P. Janasik, M. Banasiewicz, D. Mierzwa, W. Gadomski, T. D. Lohrey, J. A. Clark, M. Łapkowski, B. Kozankiewicz, V. I. Vullev, A. L. Sobolewski, P. Piatkowski and D. T. Gryko, *Chem. Sci.*, 2021, **12**, 15935-15946.
12. W. Rodríguez-Córdoba, L. Gutiérrez-Arzaluz, F. Cortés-Guzmán and J. Peon, *Chem. Commun.*, 2021, **57**, 12218-12235.
13. P. B. Ghosh and M. W. Whitehouse, *J. Med. Chem.*, 1968, **11**, 305-311.
14. T. J. Penfold, E. Gindensperger, C. Daniel and C. M. Marian, *Chem. Rev.*, 2018, **118**, 6975-7025.
15. M. A. El-Sayed, *J. Chem. Phys.*, 1964, **41**, 2462-2467.
16. M. A. El-Sayed, *J. Chem. Phys.*, 1963, **38**, 2834-2838.
17. M. El-Sayed, *J. Chem. Phys.*, 1962, **36**, 573-574.
18. J. B. Derr, J. Tamayo, J. A. Clark, M. Morales, M. F. Mayther, E. M. Espinoza, K. Rybicka-Jasińska and V. I. Vullev, *Phys. Chem. Chem. Phys.*, 2020, **22**, 21583-21629.
19. V. G. Plotnikov, *Int. J. Quantum Chem.*, 1979, **16**, 527-541.
20. Y. M. Poronik, G. V. Baryshnikov, I. Deperasińska, E. M. Espinoza, J. A. Clark, H. Ågren, D. T. Gryko and V. I. Vullev, *Commun. Chem.*, 2020, **3**, 190.
21. J. P. Zobel and L. González, *ChemPhotoChem*, 2019, **3**, 833.
22. J. P. Zobel, J. J. Nogueira and L. González, *Chem. Eur. J.*, 2018, **24**, 5379-5387.
23. H. Wu, L. Gu, G. V. Baryshnikov, H. Wang, B. F. Minaev, H. Ågren and Y. Zhao, *ACS Appl. Mater. Interfaces*, 2020, **12**, 20765-20774.
24. R. López-Arteaga, A. B. Stephansen, C. A. Guarin, T. I. Sølling and J. Peon, *J. Phys. Chem. B*, 2013, **117**, 9947-9955.
25. M.-C. Chen, Y.-L. Lee, Z.-X. Huang, D.-G. Chen and P.-T. Chou, *Chem. Eur. J.*, 2020, **26**, 7124-7130.
26. A. Brown, T. Y. Ngai, M. A. Barnes, J. A. Key and C. W. Cairo, *J. Phys. Chem. A*, 2012, **116**, 46-54.
27. S. Benson, A. Fernández, N. Barth, F. Moliner, M. Horrocks, C. Herrington, J. Abad, A. Delgado, L. Kelly, Z. Chang, Y. Feng, M. Nishiura, Y. Hori, K. Kikuchi and M. Vendrell, *Angew. Chem. Int. Ed.*, 2019, **58**, 6911-6915.
28. V. D. Parker, *J. Am. Chem. Soc.*, 1976, **98**, 98-103.
29. O. F. Mohammed and E. Vauthey, *J. Phys. Chem. A*, 2008, **112**, 3823-3830.
30. Z. R. Grabowski, K. Rotkiewicz and W. Rettig, *Chem. Rev.*, 2003, **103**, 3899-4032.
31. A. T. Nielsen, A. A. DeFusco and T. E. Browne, *J. Org. Chem.*, 1985, **50**, 4211-4218.
32. H. Kotaka, G.-i. Konishi and K. Mizuno, *Tetrahedron Lett.*, 2010, **51**, 181-184.
33. M. Tasior, G. Clermont, M. Blanchard-Desce, D. Jacquemin and D. T. Gryko, *Chem. Eur. J.*, 2019, **25**, 598-608.
34. B. Dereka, A. Rosspeintner, R. Stężycki, C. Ruckebusch, D. T. Gryko and E. Vauthey, *J. Phys. Chem. Lett.*, 2017, **8**, 6029-6034.
35. A. Janiga, D. Bednarska, B. Thorsted, J. Brewer and D. T. Gryko, *Org. Biomol. Chem.*, 2014, **12**, 2874-2881.
36. L.-B. Zhao, Y.-F. Huang, X.-M. Liu, J. R. Anema, D.-Y. Wu, B. Ren and Z.-Q. Tian, *Phys. Chem. Chem. Phys.*, 2012, **14**, 12919-12929.
37. Y. Mao, M. Head-Gordon and Y. Shao, *Chem. Sci.*, 2018, **9**, 8598-8607.
38. J. C. Dobrowolski and G. Karpińska, *ACS Omega*, 2020, **5**, 9477-9490.
39. J. C. Dobrowolski, P. F. J. Lipiński and G. Karpińska, *J. Phys. Chem. A*, 2018, **122**, 4609-4621.
40. S. Dey, D. Manogaran, S. Manogaran and H. F. SchaeferIII, *J. Chem. Phys.*, 2019, **150**, 214108.
41. N. C. Baird, *J. Am. Chem. Soc.*, 1972, **94**, 4941-4948.
42. M. Baranac-Stojanović, *J. Org. Chem.*, 2020, **85**, 4289-4297.
43. G. Markert, E. Paenurk and R. Gershoni-Poranne, *Chem. Eur. J.*, 2021, **27**, 6923-6935.
44. M. Rosenberg, C. Dahlstrand, K. Kilså and H. Ottosson, *Chem. Rev.*, 2014, **114**, 5379-5425.
45. M. H. Abraham, *Chem. Soc. Rev.*, 1993, **22**, 73-83.
46. A. K. Mora, S. Murudkar, P. K. Singh, N. S. K. Gowthaman, T. Mukherjee and S. Nath, *J. Photochem. Photobiol. A: Chem.*, 2013, **271**, 24-30.
47. C. Armbruster, M. Knapp, K. Rechthaler, R. Schamschule, A. B. J. Parusel, G. Köhler and W. Wehrmann, *J. Photochem. Photobiol. A: Chem.*, 1999, **125**, 29-38.
48. G. Jones and V. I. Vullev, *Org. Lett.*, 2002, **4**, 4001-4004.
49. D. V. Petrov and W. M. Faustino, *Opt. Commun.*, 2002, **203**, 145-150.
50. M. Shkir, B. Riscob, M. Hasmuddin, P. Singh, V. Ganesh, M. A. Wahab, E. Dieguez and G. Bhagavannarayana, *Opt. Mater.*, 2014, **36**, 675-681.
51. A. Kawski, B. Kukliński and P. Bojarski, *Chem. Phys.*, 2006, **330**, 307-312.
52. A. Costela, I. García-Moreno, J. Dabrio and R. Sastre, *J. Photochem. Photobiol. A: Chem.*, 1997, **109**, 77-86.
53. R. W. Bigelow, H. J. Freund and B. Dick, *Theor. Chim. Acta*, 1983, **63**, 177-194.
54. A. Boucetta, B. Benali, A. Kadiri, F. Ghailane, C. Cazeau-Dubroca and G. Nouchi, *Spectrochim. Acta A: Mol. Biomol. Spectrosc.*, 1994, **50**, 2249-2259.
55. R. Cammi, L. Frediani, B. Mennucci and K. Ruud, *J. Chem. Phys.*, 2003, **119**, 5818-5827.
56. O. S. Khalil, C. J. Seliskar and S. P. McGlynn, *J. Mol. Spectrosc.*, 1978, **70**, 74-83.

57. V. G. Plotnikov and V. M. Komarov, *Spectrosc. Lett.*, 1976, **9**, 265-278.
58. S. Hachiya, K. Asai and G. I. Konishi, *Tetrahedron Lett.*, 2013, **54**, 1839-1841.
59. E. Lippert, *Z. Phys. Chem.*, 1954, **2**, 328-335.
60. R. Lapouyade, A. Kuhn, J. F. Letard and W. Rettig, *Chem. Phys. Lett.*, 1993, **208**, 48-58.
61. H. Görner, *Berichte der Bunsengesellschaft/Physical Chemistry Chemical Physics*, 1998, **102**, 726-737.
62. G. Gurzadyan and H. Görner, *Chem. Phys. Lett.*, 2000, **319**, 164-172.
63. H. Gruen and H. Görner, *J. Phys. Chem.*, 1989, **93**, 7144-7152.
64. H. Görner, *J. Photochem. Photobiol. A: Chem.*, 1987, **40**, 325-339.
65. H. Görner and D. Schulte-Frohlinde, *J. Mol. Struct.*, 1982, **84**, 227-236.
66. M. Megyesi, L. Biczók, H. Görner and Z. Miskolczy, *Chem. Phys. Lett.*, 2010, **489**, 59-63.
67. J. P. Malval, F. Morlet-Savary, H. Chaumeil, L. Balan, D. L. Versace, M. Jin and A. Defoin, *J. Phys. Chem. C*, 2009, **113**, 20812-20821.
68. M. Z. K. Baig, B. Prusti, D. Roy, P. K. Sahu, M. Sarkar, A. Sharma and M. Chakravarty, *ACS Omega*, 2018, **3**, 9114-9125.
69. N. Hobeika, J. P. Malval, H. Chaumeil, V. Roucoules, F. Morlet-Savary, D. Le Nouen and F. Gritti, *J. Phys. Chem. A*, 2012, **116**, 10328-10337.
70. A. K. Singh, M. Darshi and S. Kanvah, *J. Phys. Chem. A*, 2000, **104**, 464-471.
71. Y. Miki, A. Momotake and T. Arai, *Org. Biomol. Chem.*, 2003, **1**, 2655-2660.
72. B. Carlotti, F. Elisei, U. Mazzucato and A. Spalletti, *Phys. Chem. Chem. Phys.*, 2015, **17**, 14740-14749.
73. S. Ciorba, G. Galiazzo, U. Mazzucato and A. Spalletti, *J. Phys. Chem. A*, 2010, **114**, 10761-10768.
74. B. J. Laughlin, T. L. Duniho, S. J. El Homsi, B. E. Levy, N. Deligonul, J. R. Gaffen, J. D. Protasiewicz, A. G. Tennyson and R. C. Smith, *Org. Biomol. Chem.*, 2013, **11**, 5425-5434.
75. J. S. Siddle, R. M. Ward, J. C. Collings, S. R. Rutter, L. Porrès, L. Applegarth, A. Beeby, A. S. Batsanov, A. L. Thompson, J. A. K. Howard, A. Boucekkine, K. Costuas, J. F. Halet and T. B. Marder, *New J. Chem.*, 2007, **31**, 841-851.
76. L. Mencaroni, B. Carlotti, A. Cesaretti, F. Elisei, A. Grgičević, I. Škorić and A. Spalletti, *Photochem. Photobiol. Sci.*, 2020, **19**, 1665-1676.
77. B. Carlotti, A. Cesaretti, G. Cacioppa, F. Elisei, I. Odak, I. Škorić and A. Spalletti, *J. Photochem. Photobiol. A: Chem.*, 2019, **368**, 190-199.
78. S. Hachiya, K. Asai and G. I. Konishi, *Tetrahedron Lett.*, 2013, **54**, 3317-3320.
79. F. Sadiq, J. Zhao, M. Hussain and Z. Wang, *Photochem. Photobiol. Sci.*, 2018, **17**, 1794-1803.
80. J. Dhar, N. Venkatramaiah, A. A and S. Patil, *J. Mater. Chem. C*, 2014, **2**, 3457-3466.
81. Y. Sonoda, S. Tsuzuki, M. Goto, N. Tohnai and M. Yoshida, *J. Phys. Chem. A*, 2010, **114**, 172-182.
82. Y. Sonoda, W. M. Kwok, Z. Petrasek, R. Ostler, P. Matousek, M. Towrie, A. W. Parker and D. Phillips, *J. Chem. Soc. Perkin Trans 2*, 2001, 308-314.
83. M. T. Allen and D. G. Whitten, *Chem. Rev.*, 1989, **89**, 1691-1702.
84. B. E. Kohler, *Chem. Rev.*, 1993, **93**, 41-54.
85. Y. Ueda, Y. Tanigawa, C. Kitamura, H. Ikeda, Y. Yoshimoto, M. Tanaka, K. Mizuno, H. Kurata and T. Kawase, *Chem. Asian J.*, 2013, **8**, 392-399.
86. H. K. Sinha and K. Yates, *J. Chem. Phys.*, 1990, **93**, 7085-7093.
87. J. Dobkowski, J. Herbich, J. Waluk, J. Koput and W. Kühnle, *J. Lumin.*, 1989, **44**, 149-160.
88. J. S. Zugazagoitia, C. X. Almora-Díaz and J. Peon, *J. Phys. Chem. A*, 2008, **112**, 358-365.
89. E. Collado-Fregoso, J. S. Zugazagoitia, E. F. Plaza-Medina and J. Peon, *J. Phys. Chem. A*, 2009, **113**, 13498-13508.
90. P. B. Ghosh and M. W. Whitehouse, *Biochem. J.,* 1968, **108**, 155-156.
91. S. Uchiyama, T. Santa, N. Okiyama, T. Fukushima and K. Imai, *Biomed. Chromatogr.*, 2001, **15**, 295-318.
92. S. Uchiyama, T. Santa, T. Fukushima, H. Homma and K. Imai, *J. Chem. Soc. Perkin Trans 2*, 1998, 2165-2173.
93. S. R. Norris, C. C. Warner, B. J. Lampkin, P. Bouc and B. VanVeller, *Org. Lett.*, 2019, **21**, 3817-3821.
94. C. Wang, H. J. Koh, Z. Xu and X. Liu, *Results in Chemistry*, 2021, **3**, 100116.
95. M. Echeverri, I. Martín, A. Concellón, C. Ruiz, M. S. Anselmo, E. Gutiérrez-Puebla, J. L. Serrano and B. Gómez-Lor, *ACS Omega*, 2018, **3**, 11857-11864.
96. S. Uchiyama, T. Santa and K. Imai, *J. Chem. Soc. Perkin Trans 2*, 1999, 2525-2532.
97. S. Saha and A. Samanta, *J. Phys. Chem. A*, 1998, **102**, 7903-7912.
98. F. Qian, C. Zhang, Y. Zhang, W. He, X. Gao, P. Hu and Z. Guo, *J. Am. Chem. Soc.*, 2009, **131**, 1460-1468.
99. M. Sarkar, S. Banthia, A. Patil, M. B. Ansari and A. Samanta, *New J. Chem.*, 2006, **30**, 1557-1560.
100. M. Onoda, S. Uchiyama, T. Santa and K. Imai, *Anal. Chem.*, 2002, **74**, 4089-4096.
101. M. Onoda, S. Uchiyama, A. Endo, H. Tokuyama, T. Santa and K. Imai, *Org. Lett.*, 2003, **5**, 1459-1461.
102. A. Bolduc, Y. Dong, A. Guérin and W. G. Skene, *Phys. Chem. Chem. Phys.*, 2012, **14**, 6946-6956.
103. M. Maus, W. Rettig, D. Bonafoux and R. Lapouyade, *J. Phys. Chem. A*, 1999, **103**, 3388-3401.
104. R. Ghosh, A. Nandi and D. K. Palit, *Phys. Chem. Chem. Phys.*, 2016, **18**, 7661-7671.
105. M. Krzeszewski, D. Gryko and D. T. Gryko, *Acc. Chem. Res.*, 2017, **50**, 2334-2345.
106. M. Tasior, O. Vakuliuk, D. Koga, B. Koszarna, K. Górski, M. Grzybowski, Ł. Kielesiński, M. Krzeszewski and D. T. Gryko, *J. Org. Chem.*, 2020, **85**, 13529-13543.
107. D. H. Friese, A. Mikhaylov, M. Krzeszewski, Y. M. Poronik, A. Rebane, K. Ruud and D. T. Gryko, *Chem. Eur. J.,* 2015, **21**, 18364-18374.
108. R. Stępzycki, M. Grzybowski, G. Clermont, M. Blanchard-Desce and D. T. Gryko, *Chem. Eur. J.*, 2016, **22**, 5198-5203.
109. M. Krzeszewski, K. Sahara, Y. M. Poronik, T. Kubo and D. T. Gryko, *Org. Lett.*, 2018, **20**, 1517-1520.
110. Ł. G. Łukasiewicz, H. G. Ryu, A. Mikhaylov, C. Azarias, M. Banasiewicz, B. Kozankiewicz, K. H. Ahn, D. Jacquemin, A. Rebane and D. T. Gryko, *Chem. Asian J.*, 2017, **12**, 1736-1748.
111. Ł. G. Łukasiewicz, M. Rammo, C. Stark, M. Krzeszewski, D. Jacquemin, A. Rebane and D. T. Gryko, *ChemPhotoChem*, 2020, **4**, 508-519.

112. B. Dereka, A. Rosspeintner, M. Krzeszewski, D. T. Gryko and E. Vauthey, *Angew. Chem. Int. Ed.*, 2016, **55**, 15624-15628.
113. J. O. Morley, *Int. J. Quantum Chem.*, 1993, **46**, 19-26.
114. S. Samori, S. Tojo, M. Fujitsuka, E. L. Spitler, M. M. Haley and T. Majima, *J. Org. Chem.*, 2007, **72**, 2785-2793.
115. J. A. Marsden, J. J. Miller, L. D. Shirtcliff and M. M. Haley, *J. Am. Chem. Soc.*, 2005, **127**, 2464-2476.
116. M. Grzybowski and D. T. Gryko, *Adv. Opt. Mater.*, 2015, **3**, 280-320.
117. K. Gutkowski, K. Skonieczny, M. Bugaj, D. Jacquemin and D. T. Gryko, *Chem. Asian J.*, 2020, **15**, 1369-1375.
118. M. Vala, J. Krajčovič, S. Luňák Jr, I. Ouzzane, J.-P. Bouillon and M. Weiter, *Dyes Pigm.*, 2014, **106**, 136-142.
119. K. Skonieczny, I. Papadopoulos, D. Thiel, K. Gutkowski, P. Haines, P. M. McCosker, A. D. Laurent, P. A. Keller, T. Clark, D. Jacquemin, D. Guldi and D. T. Gryko, *Angew. Chem. Int. Ed.*, 2020, **59**, 16104-16113.
120. B. Sadowski, M. F. Rode and D. T. Gryko, *Chem. Eur. J.*, 2018, **24**, 855-864.
121. I. J. Palmer, I. N. Ragazos, F. Bernardi, M. Olivucci and M. A. Robb, *J. Am. Chem. Soc.*, 1993, **115**, 673-682.
122. A. L. Sobolewski, C. Woywod and W. Domcke, *J. Chem. Phys.*, 1993, **98**, 5627-5641.
123. J. Yang, X. Zhu, J. P. F. Nunes, J. K. Yu, R. M. Parrish, T. J. A. Wolf, M. Centurion, M. Gühr, R. Li, Y. Liu, B. Moore, M. Niebuhr, S. Park, X. Shen, S. Weathersby, T. Weinacht, T. J. Martinez and X. Wang, *Science*, 2020, **368**, 885-889.
124. W. Domcke and A. L. Sobolewski, *Science*, 2020, **368**, 820-821.
125. R. A. Marcus, *Angew. Chem. Int. Ed. Engl.*, 1993, **32**, 1111-1121.
126. V. Balzani, P. Piotrowiak, M. Rodgers, J. Mattay and D. Astruc, *Electron transfer in chemistry*, Wiley-VCH Weinheim, 2001.
127. M. R. Wasielewski, *Chem. Rev.*, 1992, **92**, 435-461.
128. D. Escudero, *Acc. Chem. Res.*, 2016, **49**, 1816-1824.
129. G. L. Closs and J. R. Miller, *Science*, 1988, **240**, 440-447.
130. D.-Y. Yang, Y.-S. Chen, P.-Y. Kuo, J.-T. Lai, C.-M. Jiang, C.-H. Lai, Y.-H. Liao and P.-T. Chou, *Org. Lett.*, 2007, **9**, 5287-5290.
131. W.-C. Lin and D.-Y. Yang, *J. Org. Chem.*, 2013, **78**, 11798-11806.
132. J. Hu, B. Xia, D. Bao, A. Ferreira, J. Wan, G. Jones and V. I. Vullev, *J. Phys. Chem. A*, 2009, **113**, 3096-3107.
133. G. Jones, D. Yan, J. Hu, J. Wan, B. Xia and V. I. Vullev, *J. Phys. Chem. Lett. B*, 2007, **111**, 6921-6929.
134. A. Weller, *Z. Phys. Chem.*, 1982, **133**, 93-98.
135. D. Rehm and A. Weller, *Isr. J. Chem.*, 1970, **8**, 259-271.
136. D. Bao, B. Millare, W. Xia, B. G. Steyer, A. A. Gerasimenko, A. Ferreira, A. Contreras and V. I. Vullev, *J. Phys. Chem. A*, 2009, **113**, 1259-1267.
137. O. O'Mari and V. I. Vullev, *Curr. Opin. Electrochem.*, 2022, **31**, 100862.
138. M. Born, *Z. Phys*, 1920, **1**, 45-48.
139. C. Coulomb, *Premier et second memoire sur l'electricite et le magnetisme, ed. by AR des Sciences, Paris, France: L'Imprimerie Royale*, 1785, 569-611.
140. C. A. de Coulomb, *Histoire de l'Académie Royale des Sciences*, 1785, 569.
141. C. A. Coulomb, *Histoire de l'Académie Royale des Sciences*, 1785, **579**, 578-611.
142. L. Onsager, *J. Am. Chem. Soc.*, 1936, **58**, 1486-1493.
143. J. B. Derr, J. Tamayo, E. M. Espinoza, J. A. Clark and V. I. Vullev, *Can. J. Chem.*, 2018, **96**, 843-858.
144. G. P. Wiederrecht, W. A. Svec, M. R. Wasielewski, T. Galili and H. Levanon, *J. Am. Chem. Soc.*, 2000, **122**, 9715-9722.
145. N. I. Rtishchev, D. V. Samoilov, V. P. Martynova and A. V. El'tsov, *Russ. J. Gen. Chem.*, 2001, **71**, 1467-1478.
146. T. Ueno, Y. Urano, H. Kojima and T. Nagano, *J. Am. Chem. Soc.*, 2006, **128**, 10640-10641.
147. K. Tateno, R. Ogawa, R. Sakamoto, M. Tsuchiya, T. Otani and T. Saito, *Org. Lett.*, 2014, **16**, 3212-3215.